Copyright Warning & Restrictions

The copyright law of the United States (Title 17, United States Code) governs the making of photocopies or other reproductions of copyrighted material.

Under certain conditions specified in the law, libraries and archives are authorized to furnish a photocopy or other reproduction. One of these specified conditions is that the photocopy or reproduction is not to be "used for any purpose other than private study, scholarship, or research." If a, user makes a request for, or later uses, a photocopy or reproduction for purposes in excess of "fair use" that user may be liable for copyright infringement,

This institution reserves the right to refuse to accept a copying order if, in its judgment, fulfillment of the order would involve violation of copyright law.

Please Note: The author retains the copyright while the New Jersey Institute of Technology reserves the right to distribute this thesis or dissertation

Printing note: If you do not wish to print this page, then select "Pages from: first page # to: last page #" on the print dialog screen

ABSTRACT

CHARACTERIZING MOTOR CONTROL SIGNALS IN THE SPINAL CORD

by

Yi Guo

The main goal of this project is to develop a rodent model to study the central command signals generated in the brain and spinal cord for the control of motor function in the forearms. The nature of the central command signal has been debated for many decades with only limited progress. This thesis presents a project that investigated this problem using novel techniques. Rats are instrumented to record the control signals in their spinal cord while they are performing lever press task they are trained in. A haptic interface and wireless neural data amplifier system simultaneously collects dynamic and neural data.

Isometric force is predicted from force signal using a combination of time-frequency analysis, Principle component analysis and linear filters. Neural-force mapping obtained at one location are subsequently applied to isometric data recorded at other locations.

Prediction errors exhibited negative relationship with the isometric position at upper half of movement range. This suggests the presence of restorative forces which are consistent with positional feedback at spinal level. The animal also appears to become unstable in the lower half of their movement ranges, likely caused by a transition from bipedal to quadruped posture.

The presence of local feedback and ability for animals to plan postures that are unstable in absence of external forces suggest that descending signal is a reference trajectory planned using internal models. This has important consequences in design of neuroprosthetic actuators: Inverse dynamic models of patient limbs and local positional feedbacks can improve their performance.

CHARACTERIZING MOTOR CONTROL SIGNALS IN THE SPINAL CORD

by
Yi Guo

A Dissertation
Submitted to the Faculty of
New Jersey Institute of Technology
And the Rutgers University the State University of New Jersey
in Partial Fulfillment of the Requirements for the Degree of
Doctor of Philosophy in Biomedical Engineering

Joint Program in Biomedical Engineering

May 2014

.

APPROVAL PAGE

CHARACTERIZING MOTOR CONTROL SIGNALS IN THE SPINAL CORD

Yi Guo

Dr. Richard A. Foulds, Dissertation Advisor — Date
Associate Professor of Biomedical Engineering, NJIT

Dr. Mesut Sahin, Dissertation Advisor — Date
Associate Professor of Biomedical Engineering, NJIT

Dr. Sergei Adamovich, Dissertation Advisor — Date
Associate Professor of Biomedical Engineering, NJIT

Dr. Joshua R. Berlin, Committee Member — Date
Professor of Pharmacology and Physiology, Rutgers University NJMS

Dr. Tara L. Alvarez, Committee Member — Date
Associate Professor of Biomedical Engineering, NJIT

Dr. Eugene Tunik, Committee Member — Date
Associate Professor of Rehabilitation & Movement Sciences, Rutgers University NJMS

BIOGRAPHICAL SKETCH

Author: Yi Guo

Degree: Doctor of Philosophy

Date: May 2014

Undergraduate and Graduate Education:

- Doctor of Philosophy in Electrical Engineering,
  New Jersey Institute of Technology, Newark, NJ, 2014

- Bachelor of Science in Computer Systems Engineering,
  Rensselaer Polytechnic Institute, Troy NY, 2005

Major: Biomedical Engineering

Presentations and Publications:

Han, S., Guo, Y., Granger-Donnetti, B., Vicci, V., Alvarez, T.L.. *Quantification of heterophoria and phoria adaptation using an automated objective system compared to clinical methods*
Ophthalmic Physiol Opt. 2010 Jan;30(1):95-107. doi: 10.1111/j.1475-1313.2009.00681.x. Epub 2009 Aug 13.

Guo, Y., Kim, E.H., Alvarez, T.L. *VisualEyes: a modular software system for oculomotor experimentation.*
J Vis Exp. 2011;(51): doi: 10.3791/3475.

Guo, Y., Chen L., Pfister B.J., *Automated high throughput axon injury system for the study of brain injury mechanisms.*
Program No. 647.11, Society for Neuroscience, 2008, Washington, DC.

Magou, G.C., Guo, Y., Pfister, B.J., *Engineering a high throughput axon injury system.*
J Neurotrauma. 2011 Nov;28(11):2203-18. doi: 10.1089/neu.2010.1596. Epub 2011 Oct 12.

Moustafa, A., Guo, Y. *Recall accuracy depends on connection density in mutually connected auto associative network models.*
Program No. 622.09/YY71, Society for Neuroscience, 2011, Washington, DC.

Guo, Y., Adamovich, S.V., Foulds, R.A., Sahin, M. *Neural signals related to kinetic and kinematic variables in the spinal cord.*
Program No. 697.04/OO19, Society for Neuroscience, 2011, Washington, DC.

Guo, Y., Sahin, M., Foulds, R.A., Adamovich, S.V. *Corticospinal signals recorded with meas can predict the volitional forearm forces in rats.*
Program No. ThD10.9, EMBC 2013, Osaka Japan.

Guo, Y., Sahin, M., Foulds, R.A., Adamovich, S.V. *Forearm forces encoded by corticolspinal tract signals in the rat.*
In progress

Guo, Y., Adamovich, S.V., Foulds, R.A., Sahin, M. *Evidences of positional feedbacks in rat spinal cord.*
In progress

To Karan S’jet, whose Hand Shapes What is.

ACKNOWLEDGMENT

This project was made possible by guidance from Dr. Richard A. Foulds, Sergei Adamovich and Sahin Mesut. This study was supported by NIH/NINDS grant 5R01NS072385 to Sahin Mesut and NJSCR graduate fellowship 11-2956-SCR-E-0 to Yi Guo and Richard Foulds. The project was completed with the guidance from members of the dissertation committee.

TABLE OF CONTENTS

TABLE OF CONTENTS

(Continued)

Chapter **Page**

TABLE OF CONTENTS

(Continued)

Chapter **Page**

TABLE OF CONTENTS

(Continued)

Chapter **Page**

TABLE OF CONTENTS

(Continued)

Chapter **Page**

LIST OF FIGURES

LIST OF FIGURES

(Continued)

LIST OF TABLES

CHAPTER 1

INTRODUCTION

The overall objective of this thesis project was acquiring an understanding of descending signal for voluntary movement and posture in the spinal cord via direct investigation. The overreaching goal was accomplished in three steps: Acquisition, Analysis and Interpretation. Each objective was design to have independent application while supplying necessary knowledge for the subsequent objective. This chapter will provide justifications for these goals.

Aim 1: Develop an Advanced System for Accurate Quantification of Forelimb Movement in Rats.

The initial focus of the project was to replace hand digitization previously used for this task and provide very accurate measurements for hypothesis testing. This technology must be modular so that it may be adopted by laboratories interested in making similar measurement. The forelimb movements must be perturbed to study the command control signals during experimental trials. This will be achieved through the control of the forces applied to the end effector, using a programmable actuator known as a haptic device. In addition to applying a force, the haptic device can also measure its position and rotation in space. The device would also be engineered to include sensors that precisely measure force and torque in multiple directions. This aim was expected to provide physiological measurement such as end effector force and position for aim three.

Aim 2: Record Command Signals from Spinal White and Gray Matter

Chronic recording in the dorsal funiculus was achieved previously using planar arrays. Trauma to the tissue was observed during those studies. Other type of electrodes will be tested for their ability to produce stable recording. Both white (descending axonal tracts) and gray matter (neuronal circuitry in the spinal segments) signals was to be recorded to gain insights about how the descending signals are processed in the spinal cord neural circuitry. Post synaptic potentials in the grey matter were expected to contain lower frequency content than white matter. This measurement was expected to provide neural activity measurement for aim three.

Aim 3: Develop a Model of Central Control for the Motor Function

The electrodes would collect field potentials from an area populated with axons. It is only necessary for some component of the descending signal to represent a variable of interest. Appropriate algorithms would be selected to separate signals present in the raw data and identify the relevant sources. Tests would be conducted on measured and predicted forces under a variety of conditions in order to draw conclusions on the nature of descending signal.

1.1 Acquisition

Haptic force feedback devices simulate tactile environments by generating forces dependent on position and velocity of a manipulator. They can simulate characteristics of different mediums such as oil and water, or arbitrary shapes in space. Haptic systems also stimulate perturbations of a movement. These devices were instrumental in studies of motor planning in human subjects (need reference). For example, insights in motor learning obtained by training subjects to compensate for persistent biasing forces (e.g., a constant force normal to direction of travel) and understanding of feedback mechanisms were obtained by observing trajectories movements after brief perturbations.

Rodents are more economically advantageous compared to primates. Availability of neural signals can help in reducing ambiguity in interpretation of movement data. The ability to repeat invasive experiments makes rodents an attractive choice when effective duration of recording is limited by tissue responses.

One conventional method is to have rodents press spring loaded levers in behavioral tests [1]. However, these experiments provide limited insights for movement planning. For a spring loaded lever, the position is always related to force by a constant. Applicability of such a system is limited. For instance, it cannot be used to determine if the neuromuscular system produces position-dependent force because the force generated by a lever is a linear function of position.

In order to study motor planning in the context of neural command signals, a system was developed to perform haptic experiments on trained rodents. The system simultaneously collects synchronized neural signals. The system was designed to be

flexible enough to be configured for several types of experiments including basic lever press, viscous lever press and halting experiments.

1.2 Analysis

Severe injuries at the cervical spinal cord can result in quadriplegia due to extensive paralysis of the body below shoulders. The brain-computer interfacing (BCI) is a technique to substitute for the lost command signals in these severely paralyzed individuals, using the neural signals recorded in the brain. Brain-computer interfaces attempt to 'read' the volitional information from various cerebral cortices, primarily those involved in planning and execution of the motor function. A large number of microelectrodes implanted in the brain parenchyma record single spike activity of local neurons to extract the volitional information. However, three decades of research has repeatedly concluded that stable recordings of individual cell activities with microelectrodes have many technical challenges. The most significant problem is the layer of activated astrocytes that forms around the recording electrode and makes it very difficult to follow single spikes over an extended period of time [2]. Attempts have also been made to characterize the local field potentials and cortical surface recordings with non-penetrating electrodes as a source of volitional information [3, 4].

Looking at the big picture, the final pathway for all the motor control information processed in the brain is the descending tracts of the spinal cord before the signals reach the skeletal muscle. The corticospinal tract (CST) and the rubrospinal tract (RST) together make up the lateral descending system that controls the muscles of the extremities in all the mammals [5]. These two tracts work synergistically [6, 7], although the relative importance of each may be different in different species. For instance, the

magnocellular portion of the red nucleus, where the RST originates [8], is larger and thus suggesting a greater role in rodents than it is in primates [9] The RST was reported to have a larger effect on the finger extensors than the CST in the rat [6] Unilateral lesioning experiments of the medullary pyramid in rats impaired rotatory movements in the contralateral arm including limb aiming, pronation and supination but spared limb advancement, digit opening, arpeggio and grasping [7]. The red nucleus lesions, in addition to producing similar impairments in rotatory movements, also attenuated arpeggio. Both lesions affected both proximal and distal musculature, however, even after combined lesions the rats were able to advance the limb, grasp food and withdraw the limb [7], suggesting that some components of skilled limb use are supported by descending neural pathways or spinal cord circuits other than the crossed RST or CST. Whishaw et al. [7] concluded that rats with pyramidal tract lesions were more impaired in limb guidance than rats with red nucleus lesions, however the relative contributions of each tract were reversed in the control of the wrist and digits. In support of the importance of the CST in the rat, a recent study showed that the supination of the hand while reaching for a vertical bar was lost after a contralateral pyradoctomy [10]. Thus, the current research collectively suggests that both CST and RST are recruited in rats synergistically in the control of the forelimbs in a complementary way although the relative importance of each may be different depending on the behavioral context.

The nature of the control information descending via the CST is not known perhaps due to technical difficulties in neural recordings directly from the tract in experimental animals. Instead, indirect observations are made though micro stimulation of the motor cortex in animals or transcranial magnetic stimulation in human subjects

where the modulatory effect of CST is seen on the corresponding muscle activities. Micro stimulation of the primary motor cortex in rhesus macaques generated both facilitatory and suppression effects in both flexor and extensor muscles of the distal and proximal forearm [11]; which is a response presumably mediated through the corticospinal tract. Transcranial magnetic stimulation of the supplementary and primary motor areas during isometric static hand force task produced EMG effects with similar amplitude and latencies recorded from the intrinsic hand muscles, suggesting that both cortical areas effectively control the spinal cord excitability [12]. Indeed, many areas of the neocortex send projections to the spinal cord through the CST. Another method of gleaning information about the CST function during behavior is to correlate the single cell activity recorded from a brain region or scalp EEG and the muscle EMG signals. Frequency-domain analysis in humans has shown that isometric muscle contractions at submaximal voluntary force levels are characterized by EEG-EMG synchrony in the 15-30Hz band [13, 14]. This synchronization diminishes during dynamic muscle contractions and gets replaced by a higher frequency band around 30-60Hz [15]. The postspike facilitation studies in awake monkeys demonstrated that the tonic discharges related to the static limb torque were more prominent in the corticomotoneurons, cortical neurons that synapse on the spinal motor neurons, in contrast to the rubromotoneuronal cells [16, 17].

The number of fiber counts in the medullary pyramid varies between 73,000-150,000 in the rat (depending on whether light or electron microscopy is used [18-20]). Most of the fibers are slow conducting with diameters less than 1 µm with the largest ones around 3.7 µm [21]. Being located in the most ventral side of the dorsal column of the rat spinal cord, the fine fibers of the CST can readily be contrasted with the large

fibers of the more superficially placed ascending pathways of the dorsal column. The fast fibers reaching up to the speed of 19 m/s [22], and presumably the largest ones, are very small in number in the rat CST [23].

As an alternative approach to the Brain Computer Interfaces (BCIs), the lateral descending tracts of the spinal cord may be a potential site for tapping into volitional motor signals. Due to the convergence of the cortical outputs into a final common pathway in the descending tracts of the spinal cord, neural interfaces with the spinal cord have a potential of being more compact than the BCIs because the cell bodies of upper motor neurons are dispersed over the cortex. It is interesting to note that complete ablation of the sensorimotor cortex led to the loss of only about 50% of the axons in the medullary pyramid in rats, suggesting that remaining 50% of the myelinated axons come from areas other than the sensorimotor cortex. In light of what is known about the CST, It can be asserted that multi-electrode recordings made in this tract will be able to extract the volitional motor information in behaving animals. As in the cortical approaches, the mechanical stability of the recording electrodes in the spinal cord is crucial for those source weights to be stable over time.

Both CST and RST neurons are known to survive spinal cord injuries.[24-26] After an injury Wallerian degeneration occurs in the axons distal to the injury. Stumps proximal to axon injuries often survive the injury and sprout growth in order to bridge the lesion. In CNS regenerative processes are impeded because Oligodendrocytes has difficulty surviving in the absence of axons. For this reason it is reasonable to assert that spinal cord injuries will have minimal impact on the quality of recording performed proximal to the injury.

In previous work by Abishek and Sahin, recordings from the rubrospinal tract (RST) were found to be stable in signal amplitudes, but cross validation of regression coefficients for the forelimb kinematics between multiple trials was not successful [27, 28]. The poor reproducibility of the regression coefficients was most likely to be caused by mechanical instability of the electrode interface, the wire and Utah array electrodes. It was then decided to test a flexible substrate, planar electrode array for this application. An electrode assembly with a stainless steel supporting frame was developed to restrict the movement of the array in the cord and extend the lifetime of the interconnecting ribbon cable that runs to the external connector. The well-defined positions of the contacts in the array also permitted sampling of the tract more uniformly than the wire electrodes.

In this study, neural signals were collected from rats trained for the lever pressing task in order to assess the feasibility of extracting volitional motor signals from the CST. The level of success in predicting the forelimb isometric forces using the neural signals were comparable to that of BCI studies. Partial results were published as a conference paper [29].

1.3 Interpretation

1.3.1 Understanding Representation of Descending Spinal Signals

Any neural-prosthetic device intended to restore voluntary movement to patients suffering from paralysis must perform one of the two functions. They must either transmit properly encoded command signal to correct recipients to bypass the lesion [30, 31] or interpret this signal in order to drive robotic actuators. In both cases, an understanding of neural coding of motor control is necessary.

Extensive human studies were carried out in order to determine the control mechanism of voluntary movements. Two apparently contradictory school of theories were developed on these results. Due to the inclonclusive nature of the discussion on this topic, this study was designed to determine the nature of descending command signal by direct investigation.

1.3.2 Controversy on Control Mechanisms

There has been a long-standing controversy regarding how the central nervous system plan and execute voluntary movements. There are two main school of theory on this topic. The first school - Inverse dynamic control, postulates that CNS calculates forces required to execute a movement prior to the movement.[32] And the second school, Equilibrium control theory - speculate that cortex and cerebellum generates a reference trajectory that is followed by local feedback to produce the movement. [33] There is compelling evidence for either school of thought.

1.3.3 Internal Dynamic Models

It was demonstrated that a subject operating in a force field that constantly applied disruptive force in one direction will generate grossly distorted trajectories. [34] The subject will learn to compensate for the field over time, and will continue to compensate for the field for a time after it's turned off. This suggests that motor learning plays an important role in the planning and execution of movements.

A number of related study suggested motor learning refines internal forward and inverse dynamic models in the cerebellum. [35-37] Forward dynamic models predict

outcomes of command signals and inverse models calculate necessary command signals to generate a movement. Pairs of forward and inverse models working in conjunction allow predictive correction of command signal by Efference copy. [38] Using a copy of the command signal send to the periphery, the internal models can anticipate error in execution of movements and correct them preemptively.

In his 1996 paper, Mitsuo Kawato argued that Equilibrium trajectory cannot resemble physical trajectory in reaching movements. [39] This was derived in an experiment that measured position and stiffness of end effectors of human subjects performing reaching movements. Possible Reference trajectory was estimated using physical trajectory and measured stiffness. This trajectory did not resemble the physical trajectory. [40]

This result was sometimes interpreted as the CNS specifies force [41, 42], which leads to the controversies described above. However it only contradicts a descending reference trajectory that resembles a physical trajectory. Internal dynamic models can co-exist with a descending virtue trajectory [43]. It is possible for internal dynamic models to modify the reference trajectories to generate desired force [44]. For instance, when human subjects generating a fixed amount of isometric force using a single finger were suddenly unloaded, the finger will displace a distance proportional to the intended force until corrected.

1.3.4 Equilibrium Control

Observations were made that a force abruptly applied for a short period during a movement does not affect the final position of it. [45] [46]This suggests that some feedback mechanism must exist at spinal level to rapidly restore a perturbed movement because there is no time for intervention from cortex or cerebellum.

It was suggested that this is same stretch reflexes that stabilizes postures in stationary vertebrates. [47-49] If this was not the case, the final posture after a movement would be unstable, the postural mechanism would revert animals to their original posture after completion of movements.

1.3.5 Coordinate Invariance of the Reference Trajectory

This investigation deals only with the potential for kinetic or kinematic coding of descending signals. It does not address the possibility of muscle force vs. joint moment, or the alternatives of joint or Cartesisian kinematics.

A number of stimulation studies hinted that movements are constructed by combination of force fields that defines point attractors and limit circles. [50-54] While the coordinate system is abstract, it's possible to define the behavior on biological end effector as a potential field defined in three dimensional space.

It has been mathematically determined that if a function defines a potential field over a three dimensional space, the potential field remain the same regardless the coordinate system used to describe the space [55]. According to Equilibrium control theory, any given combination of descending signal defines the potential field of end effectors. Therefore the equilibrium trajectory can be written in muscular, joint or end

effecter coordinates [56]. This invariance does not hold true for force command signals because they do not form a potential field.

1.3.6 Direct Investigation of Descending Neural Code

This work does not seek to support or deny either mechanism for planning movement. This controversy could be the consequence of coexistence of both internal model and reference trajectory. The effects of cortical control loop can be eliminated by extraction of command signal in the spinal cord. By predicting force using spinal signals, it is possible to implement experiments without assumptions of intentions.

When examined as a whole a closed looped system including the muscle, spinal cord and the brain may appear to be regulating force when it internally accomplishes this by modification of a positional trajectory. A direct investigation of the descending signal has sufficient finesse to analyze such a system.

Recent Advances in recording techniques had opened avenues for such investigations [27, 28] . The current study uses a haptic experiment designed for rodents to investigate the properties of descending command signal, taking advantage of possible coordinate-invariant nature of possible descending trajectories.

CHAPTER 2

EFFICIENT IMPLIMENTATION OF

HAPTIC EXPERIMENTS FOR RODENTS

2.1 Method

2.1.1 Modular Instrumentation

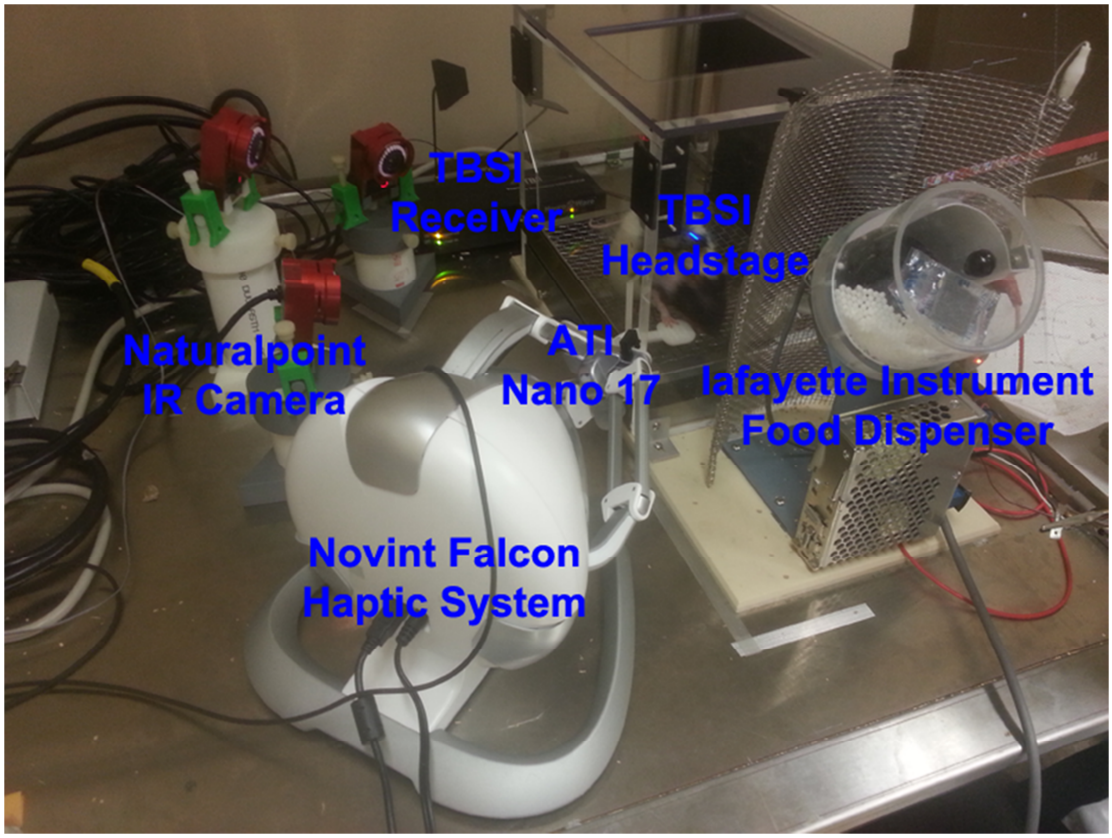

Figure 2.1 A picture of The DAQ system in operation.

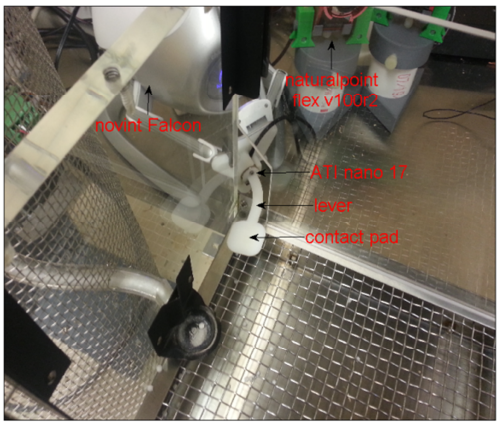

Figure 2.2 A photo of the Falcon haptic manipulator with the force sensor (Nano 17, ATI) and custom-design lever installed into a transparent training box. The picture shows the corner of the box from inside where a window was opened through which the lever arm was brought in. The rats are trained to push down on the contact pad with their preferred hand. The lever is switched to the opposite side of the box for a left-handed animal.

The cage was designed to be as optically transparent and resistant to cracks. This was accomplished by using brackets instead of screws to secure non-load-bearing elements. An added benefit was that the cage could be quickly reassembled in various configurations for different experimental paradigms.

The cage was built around two 20mm cast acrylic load bearing panels secured to a plastic base via brackets. A horizontal strip of Brass connected the two panels and anchored the stainless steel mesh floor and tray beneath it. The tray and mesh floor are interchangeable with components from Lafayette instrument modular cages.

Two vertically oriented brackets were attached to corners at the top of both load-bearing panels. These brackets hold in place 6mm interchangeable cast acrylic side panels. Two holes were drilled into the top surface of each 20mm panel to allow for the roof to be adjusted. The roof was constructed from two 6mm polycarbonate panels separated by vertical polycarbonate strips. The height of interior space of the cage can be changed by moving hex nuts that slide along four screws. The adjustable roof was interchangeable with a standard roof panel that had an opening to accommodate tethered recording systems.

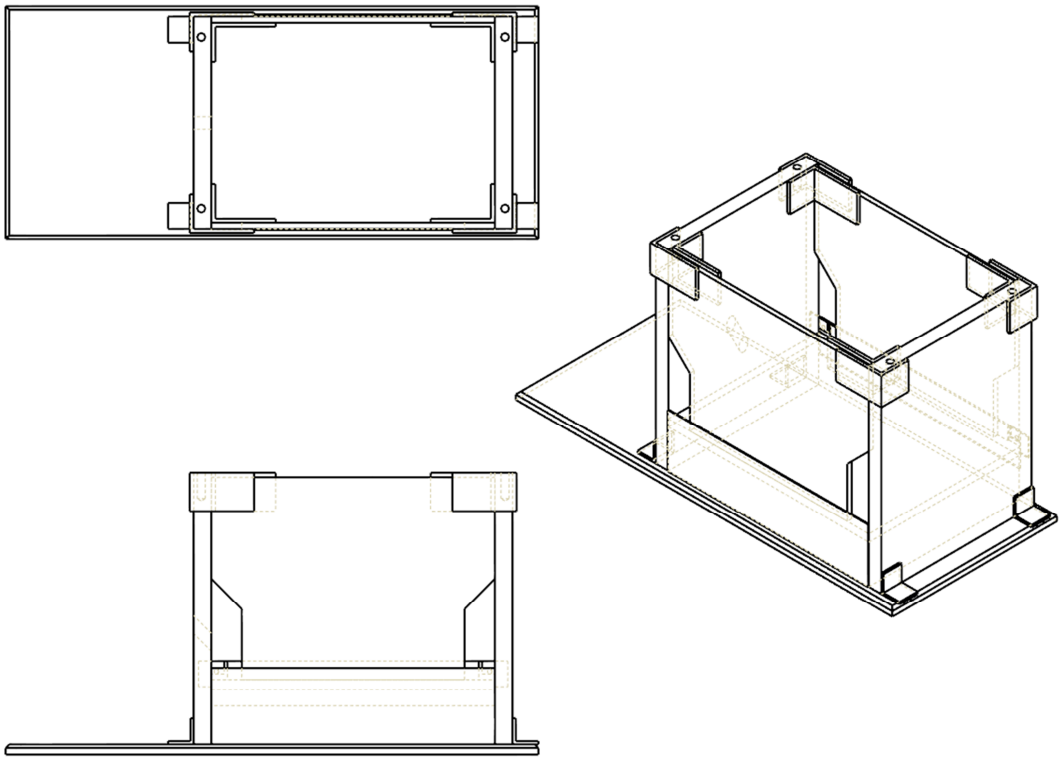

Figure 2.3 Assembly schematics of the experimental cage.

Both the load-bearing panels were made from transparent material (what type) to facilitate imaging. The side panels were interchangeable because infrared LED on high speed cameras cast reflections that interfere with tracking. Reflection on the near wall could be eliminated with adaptation filtering (see Section 2.1.4), but reflections that are periodically obstructed by the animal cannot. A panel painted chalkboard black served as backdrop that reduced reflections so it was negligible.

Falcon haptic force feedback devices were used in the study. The handle was modified into a level and a force transducer was integrated into it. Modified handles were sculpted from ABS plastic using a 3D scan performed on the original. A piece of brass at the back of the handle connected the second contact on both sides and allowed the falcon to recognize the modified lever.

The spherical handle was modified into a cylindrical socket mount for ATI Nano 17 force/torque transducers. The transducer was kept in place by friction generated via four radially placed screws. Levers were also sculpted from ABS plastic and mounted to the force transducer using a trio of screws.

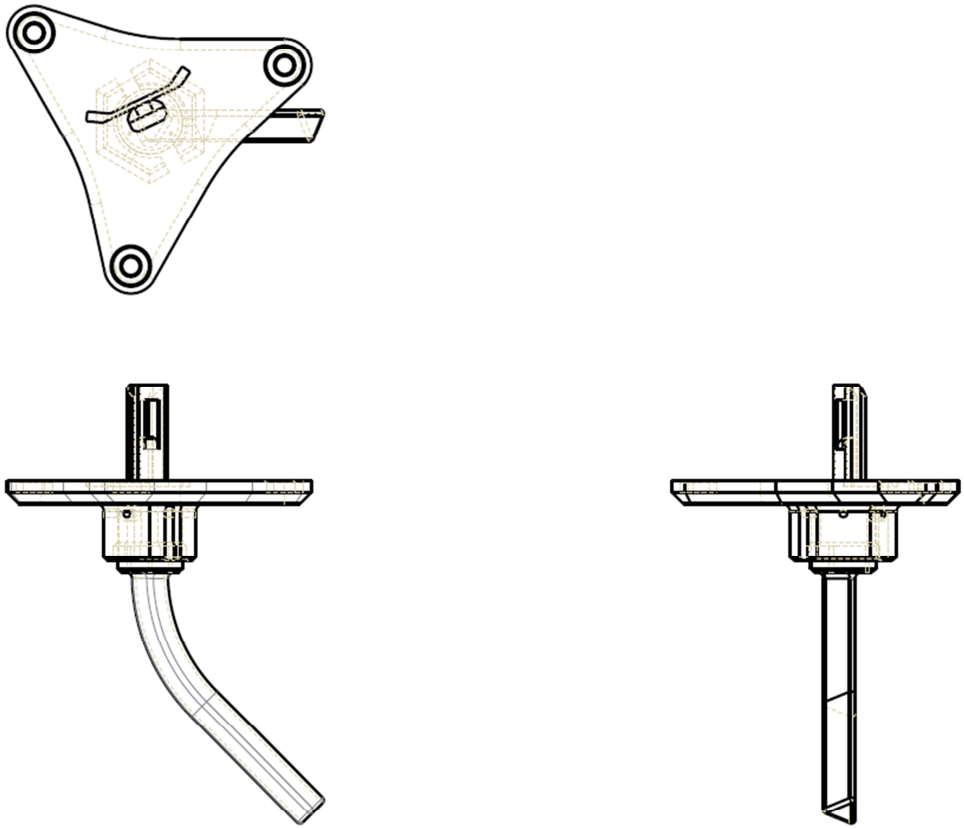

Figure 2.4 Assembly schematics for the lever.

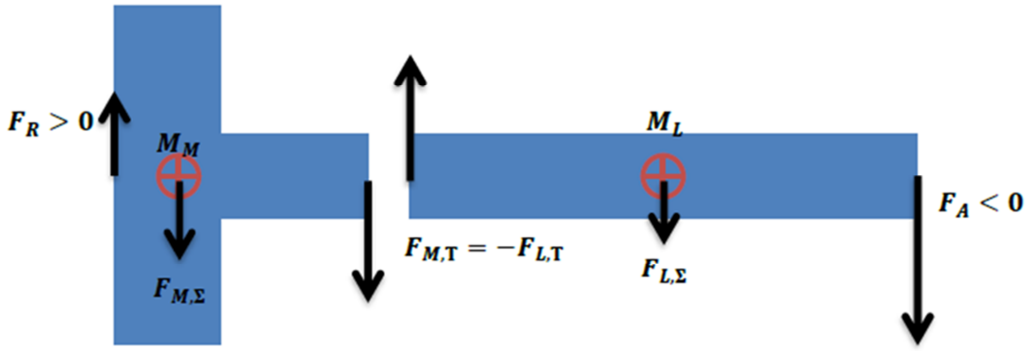

$\boldsymbol{F_R}$ Is the force exerted by the haptic device. $\boldsymbol{F_A}$is the force exerted by the animal.
$\boldsymbol{F_{M,\Sigma}}$ Is the sum of force on the mount. $\boldsymbol{F_{L,\Sigma}}$ is the sum of force on the lever.
$\boldsymbol{F_{M,T}}$ and $\boldsymbol{F_{L,T}}$ are the forces measured by the transducer.
$\boldsymbol{M_M}$ is the mass of the mount and the tranducer and
$\boldsymbol{M_L}$ is the mass of the lever.

The analysis assumes that the acceleration on both components must be identical.

$$\Delta = \frac{F_A + F_R}{M_M + M_L} + g$$

Therefore

$$F_{M,\Sigma} = \left(\frac{F_A + F_R}{M_M + M_L} + g\right) M_M = F_R + F_{M,T} + M_M g$$

$$F_{M,T} = \left(\frac{F_A + F_R}{M_M + M_L} + g\right) M_M - F_R - M_M g$$

$$= \frac{F_A M_M}{M_M + M_L} + \frac{F_R M_M}{M_M + M_L} + g M_M - \frac{F_R M_M}{M_M + M_L} - \frac{F_R M_L}{M_M + M_L} - M_M g$$

$$= \frac{F_A M_M - F_R M_L}{M_M + M_L} = -F_{L,\Sigma}$$

Or that the force measured by the sensor at any given time is a weighted average of the forces exerted by the animal and the forces exerted by the haptic device. From this, one further conclusion can be drawn.

$$\lim_{M_L/M_M \to 0} F_{M,T} = \frac{F_A - F_R \frac{M_L}{M_M}}{1 + \frac{M_L}{M_M}} = F_A$$

If the lever is light compared to its mount and the transducer, the device essentially detects the force exerted by the animal.

Equation 2.1 Dynamic analysis of the lever

The default lever was curved 45 degrees to the right. This increased the area where the cameras could be positioned. An alternative lever was curved 45 degrees to the left to accommodate left handed animals.

Cameras were located atop custom mounts with three degrees of freedom. The mounts were designed so that each degree of freedom could be locked using a break controlled by a thumbscrew. This allowed cameras to be fixed at desired orientation relative to their base. Packing tape was used to mark the locations of the cameras and the cage, ensuring that their relative position and orientation did not change after calibration. The calibration method is described in Section 2.1.5.

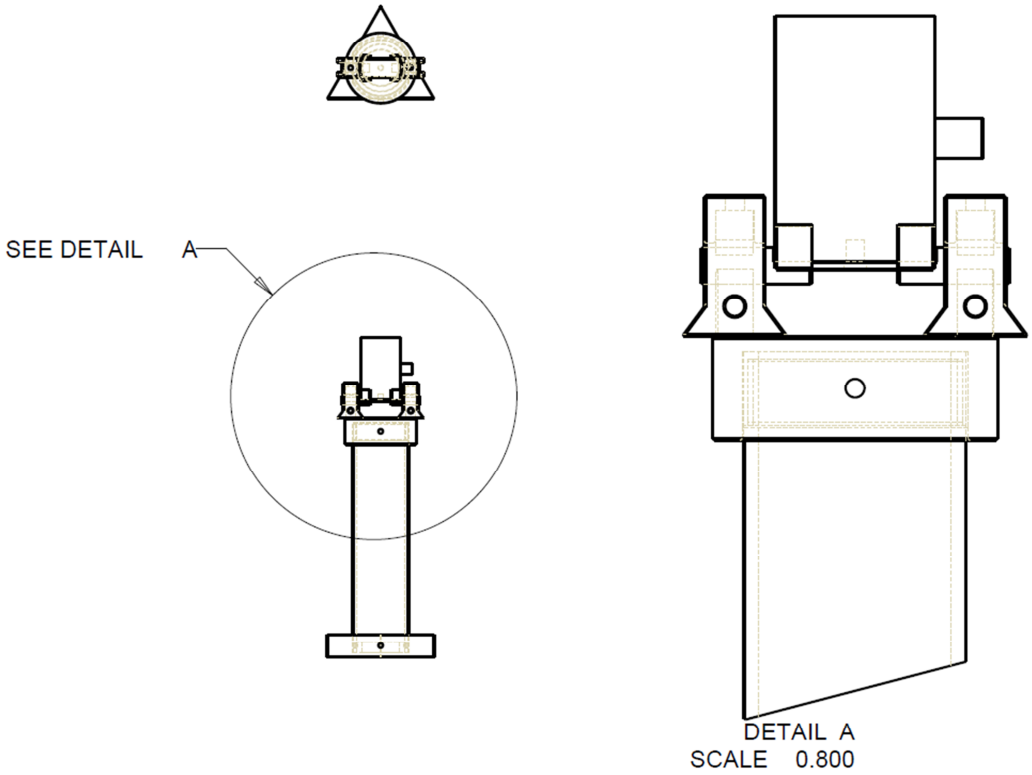

Figure 2.5 Assembly schematics for camera mounts.

2.1.2 Flexible Force Field Definition

Virtual force fields are commonly used by haptic systems to simulate a variety of tactile sensations. For example, a rigid surface can be simulated by a combination of large single sided elastic and viscous field. A weightless environment can be simulated by a negative inertial field and a constant upward force. A combination of virtual force fields defines a haptic experiment.

Force fields are functions of the three dimensional space and time relative to start of each experimental trial. To accommodate different experimental requirements, force fields are defined in a separate library and linked dynamically at run time. A library containing common fields such as elastic, viscous and inertial field was developed for lever press experiments.

Table 2.1 Force Field Export Definition Template, C++

```
#define ffexport extern "C" __declspec( dllexport )
ffexport void forcefield( const vector<float>& paramin,
const vector<float>& statesin, D3DXVECTOR3& resout );


//* paramin: force field parameters. Different type of force field has different array of parameters. See the next table for the complete list
//* statein: state of the haptic system. Defined as an array of XYZ position, followed by velocity, followed by acceleration
//* resout: force output of the force field as an array of 3 numbers corresponding to force output in 3 Cartesian directions.
```

Field Type	Parameter Definition	Output
Threshold	Lower and Upper bond for X,Y,Z and T	For each axis, 1 if device is within bond, 0 otherwise
Attractor	Attraction center for X,Y,Z and strength of the attractor	Force pointing towards the center if strength is positive
Viscosity	A single number indicating the strength of the field	A force opposing current velocity
Staticfrc	Force in X, Y, Z direction	Force specified in field defination

Composite force fields were constructed by pair-wise modulations. Each continuous field was modulated by a binary field that output either one or zero along each of the Cartesian axes. The binary field defined the region in space and time where the continuous field is active. By multiplying the output of the fields for each point in time, a field could be restricted to be active only along certain directions, within a certain range, or at a certain time. The outputs of such restricted fields were than summed to compose the desired field.

Table 2.2 Force Field Template

```
// Field template for training.
// Lever is set to InitHeight and held for InitTime.
// Then the holding field is deleted and the lever can be pushed down with minimal effort, specified by VertFrc
// The lever is halted by a virtual floor at StopHeight
// Each trial has variables replaced by their values from a row of the Variable Table

fflibary    fflib.dll
operator    pair_mod

// Triggers for record, reward and termination.
// Rat don't get food if he keeps the arm on the lever.
trigrecord  threshold  1     -1    -1    RewardHeight  1     -1    InitTime  29000
trigreward  threshold  1     -1    -1    RewardHeight  1     -1    InitTime  29000
trigendexp  threshold  -1    1     -1    1             -1    1     29001     40000
nofld

// Horizontal Restoration
field       attractor  0     0     0     256
field       threshold  -1    1     1     -1    -1    1     0     30000
field       viscosity  4096
field       threshold  -1    1     1     -1    -1    1     0     30000

// Initial Upward Displacement
field       attractor  0     InitHeight  0     256
field       threshold  1     -1    -1    1     1     -1    0     InitTime
field       viscosity  16384
field       threshold  1     -1    -1    1     1     -1    0     InitTime
field       staticfrc  0     2.0   0
field       threshold  1     -1    -1    1     1     -1    0     20

// Vertical compensation
field       staticfrc  0     VertFrc  0
field       threshold  1     -1    -1    1     1     -1    InitTime  30000

// Vertical Reistance
field       viscosity  256
field       threshold  1     -1    -1    1     1     -1    InitTime  30000

// Logical Hard Stop
// A region with ultra-high viscosity and a bit of elasticty
// viscosity cannot be too high because instability can be caused at interface.
field       attractor  0     StopHeight  0     2048
field       threshold  1     -1    -1    StopHeight  1     -1    0     30000
field       viscosity  16384
field       threshold  1     -1    -1    StopHeight  1     -1    0     30000
```

Each experimental trial was defined by a composite field. (For instance, **Table 2.2** Force Field Template shows definition of a field used in training) An experimental session contained up to 200 trials and was generated by a template with a variable table. Experimental trials were generated by a Matlab script that replaced keywords in the template with their corresponding value from the variable table. Variable tables were created by separate Matlab scripts.

Table 2.3 Segment Of Variable Table For Rising Phase

InitTime	InitHeight	RewardHeight	StopHeight	VertFrc
500	-0.017	-0.018	-0.02	-0.75
500	-0.0168	-0.018	-0.02	-0.75
500	-0.0166	-0.018	-0.02	-0.75
500	-0.0164	-0.018	-0.02	-0.75
500	-0.0162	-0.018	-0.02	-0.75
500	-0.016	-0.018	-0.02	-0.75
500	-0.0158	-0.018	-0.02	-0.75
500	-0.0156	-0.018	-0.02	-0.75
500	-0.0154	-0.018	-0.02	-0.75

For instance, during the second phase of training where the animals learned to press the lever instead of tapping it, the initial height of each trial increased successively while other parameters (such as Initial height of the lever and height at which reward is released) remain unchanged. **Table 2.3** shows a segment of the variable table used to generate this session. It was generated using a Matlab script (not shown).

2.1.3 Synchronized Data Collection

Effective analyses of neural signal required collection of a large amount of data (31 channels @ 16000Hz, or 1.89MB/S in binary format) as well as synchronization of neural, haptic and imaging data (within 1ms). DAQmx SDK was used to accomplish this. A DAQmx task was set to run continuously, and a software loop was used to transfer data to a RAM buffer for manipulation.

A DAQ device can generate more data than it is possible to write to a hard drive in real time. To overcome this, data were continuously acquired into a RAM buffer and were transferred to the hard drive after completion of each trial. In order to limit the amount of physical memory committed to this task, queue buffers were used and data were continuously removed from the back of the buffer as new data were added to the front of the buffer so they would remain a constant length until the DAQ module received a Synchronization Signal.

The synchronization signal is used to align neural, haptic and image collection treads because these tasks cannot be started instantaneously. The unpredictable amount of time it takes to start data collection tasks introduces timing errors in data collected by them. Synchronization can only be ensured by allowing data acquisition threads to run continuously and discard data to ensure the length of the buffer remain constant until the sync signal was sent.

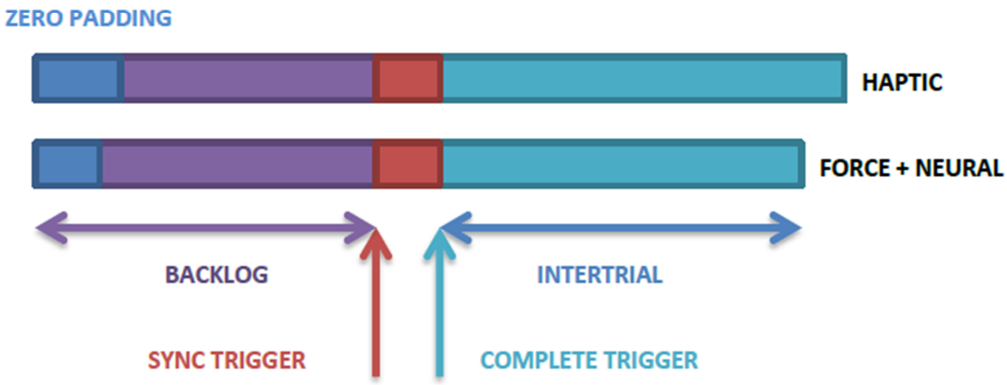

Figure 2.6 Illustration of structure of collected raw data.

Table 2.4 Recording Protocol

1. Calibrate the camera if tracking is required and cameras are not already calibrated
    a. Set Session in expconfig.txt to CamCalib
    b. Depress the lever until the first notification tone
    c. Wave the wand in front of the cameras. Ensure the marker appear in each cameral; maximize the range of motion while collecting calibration data
    d. Set calibconfig.txt, optimal configurations are determined by trial and error.
    e. Run The calibration program (SEELE.EXE)
    f. Run flipcams.m if the calibration program output cameras facing incorrectly.
2. Create DAQ task “Neural” and “Food” in Automation explorer
    a. Task “Neural” should be set to continuous acquisition, and contain analog input for both neural and force signals.
    b. Task “Food” should be set to one sample on demand, and contain analogue output channel for reward signals.
3. Set config\daqconfig.txt
    a. Ensure that the “Neural” and “Food” tasks are included in the task list.
4. Define force field configurations in config\template\template_name.txt
5. Define force field variable tables in config\template\var_name.txt; Defining variable table using matlab scripts is recommended. This step should be repeated for each randomized session.
6. Generate sessions using fldgen\fldgen.m
    a. Make sure tmpname and varname are set to the name of the template and the table
    b. Set Subject and Session to desired values
7. Set config\expconfig.txt
    a. Ensure Subject and Session matches name of the subject and session in step 6
8. Begin Data Acquisition by starting NERV.EXE
    a. To abort experiment, hit the Escape key.
    b. If the program reports an error, close the program, open task manager and look for a ghost instance of the program in the process list, and terminate it.

- See sample configuration files expconfig.txt, calibconfig.txt and daqconfig.txt in the appendix.
- Template and variable table were described in **Table 2.2** and **Table 2.3**

2.1.4 Triangulation

Naturalpoint (Corvallis, Oregon) offers a software suite that provides tracking for their camera. This suite cannot simultaneously output video and tracking data from the same camera. A custom software module was developed to simultaneously acquire both types of data. Real time processing allows tracking information to be collected at much higher rate than associated images.

Infrared LED generates strong glares when directly facing an acrylic surface. An adaptation filter was used to remove these artifacts. The adaptation filter was designed to imitate the adaptive features of human vision system. It accomplishes this by subtracting the value of each pixel with its moving average.

Table 2.5 Adaptation Filter

```
adapbyte[0] = (float(adapbyte[0]) * (1-_f->_adpcst) +
                 float(thisbyte[0]) * (_f->_adpcst))  ;

float delta = float(thisbyte[0]) - float (adapbyte[0]);
if (delta < 0) {delta = 0; }

diffbyte[0] = (unsigned char) (float(diffbyte[0]) * (1-_f->_difcst) +
                   (delta) * (_f->_difcst))  ;
```

Markers were located by finding cluster in a threshold image. It's not necessary to scan each point to locate a cluster because markers have some minimum size. By evaluating every N point in both horizontal and vertical directions, markers could be located. The extent of the marker was determined by recursive expansion from the initial point that exceeded threshold value. A queue buffer stored pixels currently being processed. Each call of the recursive expansion algorithm checks the first pixel in the buffer, if it was not already in the cluster, it was added to the cluster and removed from the image and its adjacent points were added to the queue. For each cluster, this process repeats until the queue became empty. [See Appendix B, annotated C++ Code]

2.1.5 Calibration

To calibrate the camera system, the location of the camera and the cage were marked by tape. The cage was subsequently removed and all the DOF on the camera mounts were fixed. A wand with a single marker at its tip is waved in front of the cameras while the lever was used as a switch to signal start and stop of data collection.

Single point calibrations, where the software determines relative position and orientation of the cameras from the image coordinate of a single marker in space on multiple cameras. However, this is considered an optimization problem. The goal of optimization is to minimize the sum of line distances and point distance between lines projected from possible camera location to possible marker locations.

Line distance was defined by minimal distance between two lines, and was calculated by projecting both lines onto their cross product. Point distance was defined by the sum of distances between the nearest points of each pair of lines and was calculated by projecting the lines to the plane defined by their cross product and calculating the 2D intersect. The point distance prevents the optimization from biasing towards solutions where all cameras lie on the same plane. [See Appendix B]

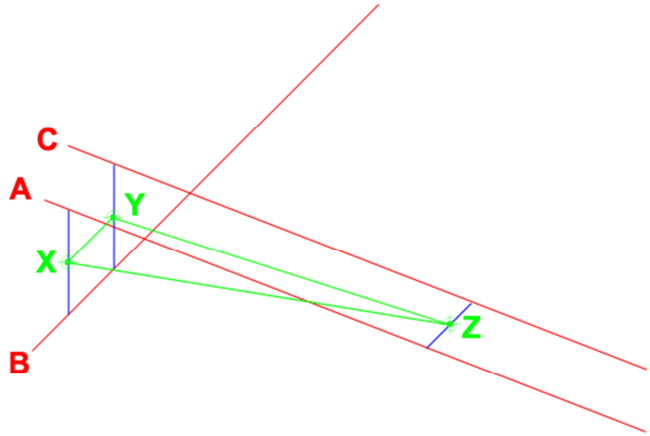

Figure 2.7 Illustration of point distances. In the illustration there are two parallel lines A and C and line B is normal to both of them. Line distance is sum of lengths of blue lines and point distances is the sum of lengths of green lines.

This optimization problem was solved by parallel gradient decent. Searches took place in a space where dimensions were camera properties (position, direction, roll and focal length). The gradients were estimated by taking a small step in each dimension and calculate the changes to the goal function. The search then takes a step in the direction of steepest gradient proportional to the current value of the goal function. This process is carried out simultaneously from hundreds of randomized initial states until a satisfactory solution was found. Such a solution position and orient cameras in such a way that each point used for calibration was represented as the same point in space with respect to all cameras.

The triangulation module also saves grayscale images as separate output. To reduce the amount of space required to store these images, they were compressed into JPEG format using a library (JPEG lib) at real time. This process was conducted using a spate thread to take advantage of multi-core CPUs.

2.1.6 Visualization

An user interface (UI) module provided real-time feedback from the DAQ system and helped the operation diagnose operational problems during the recording. The UI was functionally a statically linked library. By calling the library with arguments containing pointers, the UI module was connected to other modules. Rendering the UI was carried out by its own thread, and flag variables allow it to be disabled to avoid thread conflict caused by the UI access of the same variable at the same time as another module.

Status messages provide important update on the experiment's progress as well as any errors encountered. The UI model contained a text buffer to store status messages, as it is more efficient than attaching a text buffer to each module separately.

A Library (library specifics) was used to calculate FFT of neural signals in real time. This alerts the user of any defects in electrical connection. The library's output pointer is set to a buffer declared by the UI module. FFT was calculated after each data acquisition call; however the result was only displayed during the next render update.

The virtual force field was visualized as a vector field that changes in time. This allowed the operator to correct errors in force field definition. To ensure the visualized field is the same one simulated by the lever, the force output of the composite force field was calculated for multiple locations in 3D space during each display update.

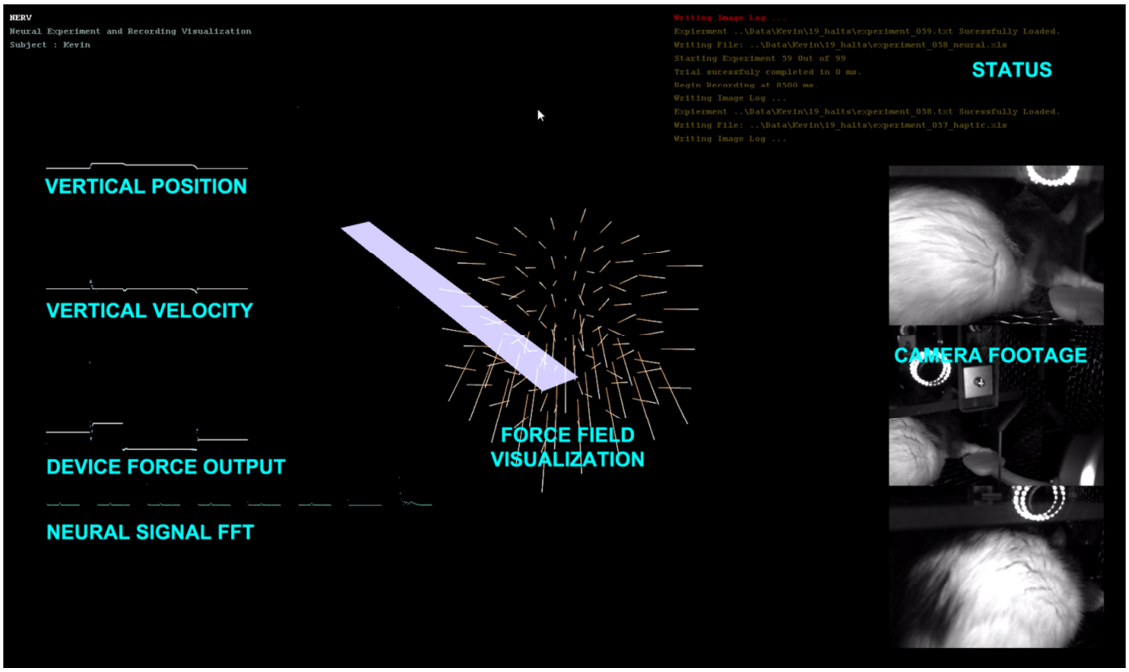

Figure 2.8 Annotated Screenshot of the DAQ system.

2.1.7 Animal Training

Rats were trained in Phases. Initially the haptic force system was programmed to release sugar pellets on contact. Rats that consistently touch the lever were moved to the next phase. In the second phase, the lever was reset to successively higher initial conditions each time. This trains the animal to press the lever for greater distances each time.

In the third phase, the amount of force required to press the lever was gradually increased. This phase is usually omitted because a large force requirement can lead to undesirable behaviors. Typically rats will press levers with one forelimb, but they will press the lever with both arms if pressing the lever with one arm becomes difficult.

In the fourth phase, the lever starts at a predetermined height in each trial. However, this training session is conducted in the presence of an adjustable roof that gradually lowered. At end of this phase the animal become accustomed to pressing the lever without standing up. The purpose of this training phase is to reduce the involvement of back muscle. Ideally movement should be restricted one single arm. This phase of training was conducted before the surgery during the experiments presented in the subsequent chapters because the collision between then antenna and the roof causes artifacts in the recording, so movement restriction were not applied to animals after their surgery.

The final phase involved slowly removing the lever from the cage so the subjects learn to press the lever by extruding an arm from the cage. However this stage is usually omitted for wireless recording because the wireless head stage collide with side panels of the cage when an animal attempts to extend its arm from the cage.

Table 2.6 Training Protocol

1. Animals should undergo acclimation as per facility guidelines
    a. Animals should be handled regularly to increase familiarity with experimenters
    b. Animals should be provided with pellets intended as reward during acclimation; This will speed up their identification during the training
2. Animals should be food restricted to 80% body weight or recommendation by guidelines.
    a. Ensure that animals are interested in the pellets before proceeding stale or unflavored pellets generate no motivation.
3. Set the system to release food upon contact, consult Data collection protocol, step 4-8
    a. The rat learns initially by accidentally colliding with the lever. Keeping the lever close to the floor of the cage increases the probability
    b. Rats prefer exploring in low-light conditions.
    c. Fresh Scent sources on the lever will encourage interaction.
    d. The animal should hit the lever consistently before moving to the next step.
4. Gradually increase the distance the rat has to move the lever.
5. Gradually increase the force required for the lever press.
    a. Mechanical viscosity for falcon is very large for a rat. Initially a downward assistive force is recommended.
    b. Very large force requirement (.6N+) encourages the animals to use both forelimbs.
6. Gradually apply movement restrictions
    a. If an adjustable roof is used, lower it over multiple days.
    b. If levers need to be outside the cage, gradually withdraw it over multiple days.
7. Perform surgery for electrode for neural signal collection.
    a. Animals must undergo a recovery period as per facility guidelines, however retraining is only required for animals that suffering neural injury.
    b. Reduced doze Antibiotics is recommended for the entire duration of the study.

2.1.8 Marker Attachments

IR Reflective markers provided Naturalpoint do not adhere to the fur, therefore additional steps had to be taken to attach them to the animals. Depilatory cream were used to remove fur from the rat's dominant arm. Spray bandages were then used to create a uniform surface the markers can attach to. This process created attachments strong enough to resist unintentional perturbations; volitionally the animals can still remove them without injury to themselves.

2.1.9 Modular Data Processing

The data processing module was written in Matlab, it was designed in stages so alteration of calculations performed at one stage does not require repetition of calculations performed at pervious stages. This greatly reduced the amount of time required to find optimal parameters (e.g., time constant, time delay, filter cutoff) by iteration.

Time-Frequency analysis is instrumental in analysis of neural signals. However, calculation of Short Time Fourier transform (STFT) requires a considerable amount of time. In order to facilitate evaluation of filters, Power Files were generated as the first step of the data processing by calculating FFT in a sliding window so filter changes did not require recalculation of power spectrums.

Power Files were filtered in the second stage of calculation. Power spectrum density were first convolved with an exponential decay function to quickly calculate a recursive average, then filtered by a low pass Butterworth filter (3rd Order butterworth 8Hz cutoff). Force values were also calculated in this stage by multiplying output of the force sensor with its calibration matrix. Optionally, the second stage also calculates power-power interaction or position-power interactions and prediction statistics.

Regression files – outputs of the second stage – were used to estimate the mapping from independent variables (position, power, interaction) to the dependent variables.. PCA (Principle Component Analysis) was carried out with all independent variables because regression only works on uncorrelated signals; De-correlated principle components were independently regressed to dependent variables. Regression coefficients of PCs were pre-multiplied by the pseudo-inverse of PCA combination matrix to produces the mapping from independent to dependent variables. See Chapter 2 for details.

When the Matlab script performing the second stage of calculations were run in the presence of a mapping file, it produced statistics for prediction performed using those mappings. This allows testing of mappings on another set of data.

Table 2.7 Data Processing Protocol

1. Recording data generate experiment_num_neural.xls, experiment_num_haptic.xls and experiment_num_imlog folders (see recording protocol)
2. Create exclude.txt (tab delimited), list trails to exclude from analysis
3. Run xform\pwrcalc.m to perform time/frequency analysis. Outputs are experiment_num_power.xls and experiment_num_force.xls
    a. Set subject to the name of the folder containing haptic and neural files
    b. Frccols should be a list force channels and nercols should list neural channels
    c. Lthw is window length in seconds, lths is the step size in seconds (1 recommended)
    d. Neufrq is the list of frequencies to be analyzed, it should be increasing
4. Copy force calibration matrix matcalfrc.xls to the folder containing output of step 3.
5. Remove existing regression.xls, samples.xls and vresult.xls from the directory
6. Delete sn_PWR_num.fig corresponding to trials of interest
7. Run unified\visualize_batch.m to perform filtering, outputs are regression.xls, samples.xls and sn_PWR_num.fig files
    a. Subject should be set to the same as step 3.
    b. Set params.fiso to 1 to include only isometric segment, -1 to exclude them
    c. nfilt.hghtau sets the time constant for the recursive average in seconds
    d. [nfilt.nb, nfilt.na] defines filter for neural data
    e. [nfilt.fb, nfilt.fa] defines filter for force data
8. Copy regression.xls, samples.xls to another folder and rename them
9. Copy electrode mapping files to the same directory, consult mapelectrode.m for details
    a. Chans.xls is a list of channel number for each ping on the connector.
    b. Cons_lefthand.xls or cons_righthand.xls is a list of contact number for each ping
    c. Eles.xls is a map of contact numbers on the electrode surface.
10. Delete weight.xls in the same directory
11. Run unified\reconstest.m to perform regression test. Outputs are figure files as well as weights.xls for the optimal weight.
    a. Regname and smpname are names for regression and sample files respectively.
    b. Colssel list columns containing dependent variables
    c. Chanfrq should match Neufrq in step 3.
12. Copy weight matrix to the original session folder containing power and force files.
13. Repeat step 5 to 7 to produce predictions, in additional to regression and sample files, an additional output file vresults.xls will be created, it will contain statistics of prediction. Consult hvalidate.m for details
14. Rename vresult.xls
15. Run stastats.m to perform the error analysis
    a. The first number sweepwin is the sigma of Gaussian window displayed on the plots; the second number is the sigma for the window used in the optimization.
    b. DC correction by subtracting median should be enabled only for controls.

- See Appendixes for example of configuration file and details of matlab scripts

2.2 Results

The capability of the system has been adequately justified by results in the subsequent chapters. In additional those results, the system has demonstrated its ability to track at least one marker. Although the complications related with tracking system limited its applicability during experiments. See section Practical Concerns of Tracking for additional details.

2.2.1 Tracking

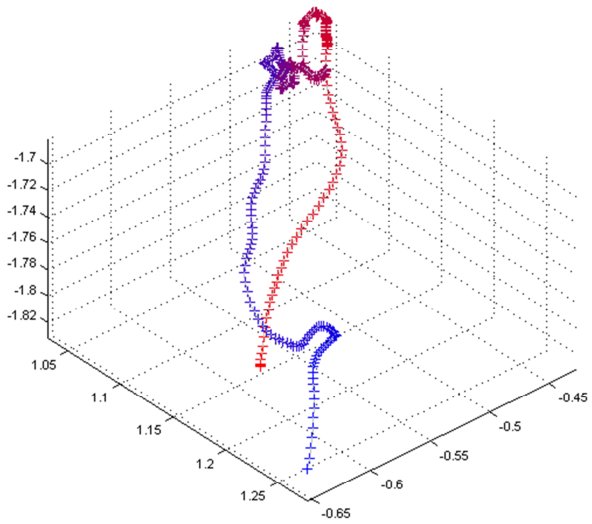

Figure 2.9 Trajectory of a single marker on the rat's shoulder during a typical lever press trial.

The Figure above shows the trajectory of a marker placed on an animal's shoulder during a lever press trial. The camera system triangulated its roughly circular motion in space at 100Hz. This is a demonstration the system was capable of production motion data if remaining issues mentioned in the following discussion section can be resolved.

2.3 Discussion

2.3.1 Software Architecture Overview

With the exception of the force field library, the DAQ and instrumentation code were implemented as static libraries linked at build time. This allows any component of the program to be replaced with libraries containing compatible interface functions. Each module has a control thread that performs the task of the module (e.g., rendering GUI, Perform Haptic or Camera Timing) according to the values of global variable of the module (e.g., GUI text list). The Global variable can then in term be set by calling interface functions or be changed in configuration files. The configuration files provide ways to configure all aspect of an experiment without modification to C++ code or recompilation.

The program could crash when multiple thread accessing the same resources for instance, when camera interface module intend to update an image that is been displayed. This problem was solved by binary local variables that can be set to indicate if a thread can proceed (e.g., GUI enable). If a control thread detects such a variable set to the disabled state, it will suspend itself, only checking that variable every millisecond until it can proceed. For instance

```
while (_add) {::Sleep (1);}
```

Multiple such variables can be used to ensure sequential execution of specific commands.

Each Control thread could spool a large number of work threads. These threads allow parallel computation on computer with multiple cores. For instance, during calibration, a separate thread was created for each step of uphill searches from each initial condition so all searches can proceed simultaneously. Work threads contain no loop, and an operating system call was used to determine their completion.

The only module that does not contain a control thread was the force field library. The force field library declares force fields as external functions. These functions could then be found and execute at run time by another module. This allows force fields to have any name, as long as their functional declaration matches the name in the force field definition file.

2.3.2 Practical Concerns of Tracking

Triangulation error causes artifacts to appear at closest point of lines projected to different points. They are difficult to eliminate without the ability to match image of a marker to the image of the same marker taken by another camera.

The tracking system encounters large errors when calibration was performed without the cage. This is due to refractive property of Acrylic. This error can be reduced by using calibration data collected with the wand inside the cage.

Additional cameras will be required to track markers at wrist and elbow. Due to motion of the animal, the markers vanished from view from one or more cameras during the lever press depending on positioning of the rat relative to the lever. This can be resolved by having more than minimum number of camera required for triangulation.

CHAPTER 3

ENCODING OF FORELIMB FORCES BY CORTICOSPINAL TRACT ACTIVITY IN THE RAT

3.1 Methodology

3.1.1 Electrode Implant

Polyimide substrate electrode arrays were custom-designed for this study (NeuroNexus, MI). The array consisted of 4x8 arrangement of 32 gold contacts with 15µm diameter and 80µm spacing. Every other column of contacts was offset with respect to the neighboring columns by 40µm to sample the CST cross sectional area more uniformly (see **Figure 3.8**). A 2×2mm PDMS sheet (127 µm thick) was attached like a collar around the MEA ribbon cable (thickness 12µm) exactly 1300µm from the tip (**Figure 3.1**). This attachment allowed precise control of penetration depth and enhanced the mechanical stability of the array by keeping it in vertical orientation in the cord.

Dorsal laminectomy was performed on C3-C4 segments under ketamine/xylazine anesthesia (80mg/kg and 12mg/kg). The modified electrode array was inserted into the dorsal column mid-sagittally with its contact side facing the preferred hand at C4. The point of entry was the posterior median sulcus of the cord and adjacent to the dorsal vein. The array was pushed into the median septum after making a small cut with a #11 blade into the pia matter. The CST occupies a region in the most ventral region of the dorsal column extending from a depth of 1000 to 1300µm measured from the pial surface in the cervical cord. The supporting PDMS attachment was slid under the dura after electrode

insertion and a small amount of cyanoacrylate was applied to the ribbon cable where it passes through the dura.

The stainless steel wireframe (Ø 0.75mm) shown in **Figure 3.1** held the electrode assembly in place. The wireframe was tied to the spinous process of C2 vertebra on the rostral side and to the C5 on the caudal end with 6.0 silk sutures. The plastic connector was fixed to the frame with dental acrylic at a height that allowed some slack in the ribbon cable to reduce tension and hence the chronic trauma to the neural tissue. The reference electrode was placed on the dura next to the electrode ribbon cable and glued in place. The neck muscles and the skin were closed in layers around the connector using fine sutures. The plastic connector was protruding ~5mm through the skin opening. The gap around the connector was sealed with further dental acrylic, which also housed the nuts for anchoring the multi-channel wireless neural amplifier.

3.1.2 Animal Training

Six Long Evans rats (350-450g) were used in this study. Food restricted rats were placed in a cage with a lever attached to a computer controlled haptic (with force feedback) device (Falcon, Novint Technologies, NM; see **Figure 2.1**). The lever was initially programmed to trigger release of 20mg sugar pellets on contact. Once the animal became familiar with the lever, the displacement required to trigger food reward was increased incrementally over time to 15mm. The animals used both hands initially to press the lever in most cases and learned to do the task with their preferred hand by training that took 1-2 weeks prior to the implant surgery. (Additional details for animal training can be found in Section 2.1.7)

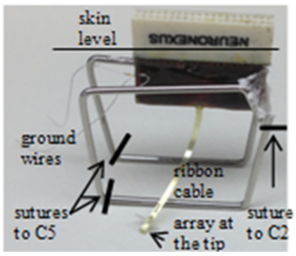

Figure 3.1 A photo of the implanted electrode/connector assembly. The electrode assembly was firmly fixed over the cervical spinal column by suturing the wire frame to vertebral bones of C2 on the rostral and C5 on the distal side.

Figure 3.2 Luxol fast blue stained transverse section of a cervical spinal cord from one of the rats. The lesion demarcates where the electrode array was implanted in the dorsal white matter. (Red arrow)

3.1.3 Data Collection

The haptic device produced 3D positional information at a rate of 1000 samples/s. A force/torque sensor (Nano 17, ATI systems) integrated into the lever measured the 3D forces applied to the contact pad at the end of the lever by the rat's arm (**Figure 2.2**).

Neural signals were amplified by a 30 channel wireless system (W32, Triangle Biosystems) before they were digitized at 16 kHz simultaneously with the force data. Infrared cameras generated video logs at 10fps for quality assessment of the behavioral task. All data streams were synchronized using custom C++ code. (See Section 2.1.3 for additional details)

Trained animals performed sessions of 50 to 200 lever presses per day until they lost interest in the sugar pellets. Trials with obvious defects were excluded from the analysis (e.g., if the operator touched the lever or the antenna came into contact with cage roof.) A rat typically produced one to two sessions of usable data before incurring damage to electrode ribbon cable. For consistency only the best session for each rat is reported.

3.1.4 Time-Frequency Analysis

Neural signals were filtered in both directions in time (to cancel phase delay) using a 3rd order Butterworth band-pass filter at 75-425 Hz (**Figure 3.3**). Any component that exceeded ±100μV in the filtered signals was considered an artifact, and upon detection 30 ms of the signal (10ms preceding to it and 20ms after) was substituted with zeros to remove it. Power spectral density was computed for each channel of filtered neural signals within a 40 ms moving window that shifted in 1 ms steps (Step B) using short time Fourier transform (STFT), which produced one Fourier coefficient per 25 Hz up to the sampling frequency of 16 kHz. Only the corresponding 13 components that represented signal power from 75 to 425 Hz were considered for further analysis. Time signals representing the power variations in 25 Hz frequency bands were generated by taking the absolute value of FFT coefficients in this moving time window (Step C). A total of 390 channels of neural power signals were formed from 30 channels of neural signals (30×13) in each trial. Both the neural signals and the forearm forces were smoothed with a 3rd order Butterworth low-pass filter (fc=8 Hz) in both directions in time to eliminate any phase lag.

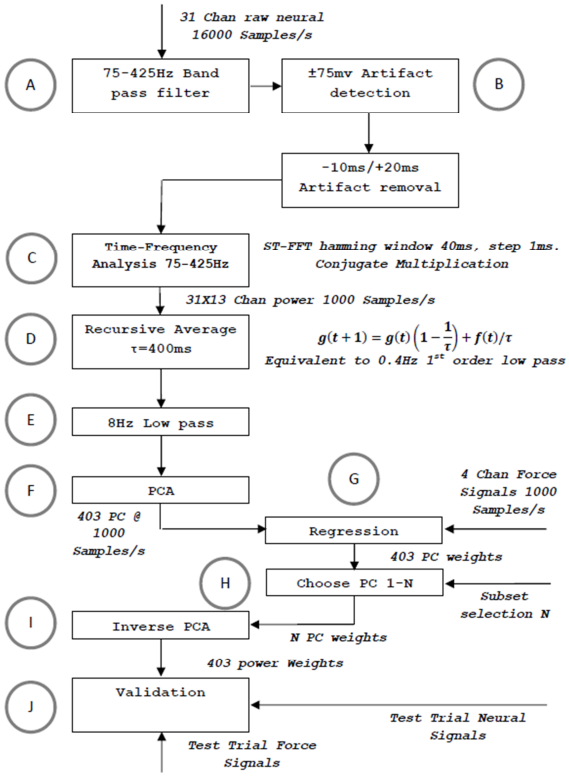

Figure 3.3 Flow chart of data processing algorithm for regression of the forelimb force in a single axis. The same algorithm was applied to all three dimensions of the force in Cartesian coordinates. See methods for details.

3.1.5 Regression and Cross Validation

The principle components (PCs) were computed and sorted in a descending order of variance. The PCs were grouped and regressed against each one of the 3-axes of the measured force as well as the magnitude of the force vector (Step G). Regression weights of PCs in each group were pre-multiplied with pseudo inverse of corresponding columns of PCA score to generate weights for power signals for the reasons below.

Let A be the transformation matrix from principle components T back to power signals$S$:

$[T] \times [A] = [S]$

$[T] = [S]/[A]$

Forces can be estimated using PCs or power signals. Here Z contain regression coefficient of principle components and W is the coefficients of power signals:

$[F] = [X] \times [W] = [T] \times [Z] = [X]/[S] \times [Z]$

Therefore weights of power signal can be calculated from weights of principle component as follows.

$[W] = [I]/[A] \times [Z]$ (3.1)

I is the identity matrix. Matrix division is used because A may not be invertible.

Every third trial in each session was held back for testing and the remaining trials were used for computation of the regression coefficients (training set). The test set data underwent the same time-frequency analysis as the training set. The weights for the power signals corresponding to each set of PCs calculated in the training set were applied to the test set. The number of PCs in the group was increased incrementally to search for the best regression coefficients. Goodness of fit was measured by both the coefficient of correlation (R) and the coefficient of determination, R-squared (**Table 3.2**), for all the trials in the set and the mean values were reported. The weights that generated the best fit to the force data were selected.

$R^2 = 1 - \frac{\sum_t (F - \hat{F})^2}{\sum_t (F - \bar{F})^2}$ (3.2)

Where the nominator is the sum of squares of prediction errors and the denominator is the variance of the measured force. $\bar{F}$, Mean of measured force. $\hat{F}$, Predicted force.

3.2 Results

Three dimensional force and position information recorded from the lever is plotted in **Figure 3.4** in a typical trial. The lever starts moving about 150ms before the isometric portion begins at 2000ms. All data channels are backlogged continuously for 2000ms until the lever press is detected. The isometric state, shown as the highlighted portion in the traces, is achieved by increasing the simulated viscosity of the medium to a very large value by the computer controlled haptic interface. The isometric vertical force (y in green) is the largest as expected for the lever pressing behavior. Nonetheless, small forces are recorded in the side-to-side (X in blue) and back-and-forth (Z in red) directions as well. The magnitude of the combined force vector (ABS) resembles that of the vertical force since it is the largest component. Isometric interval ends when the rat lifts the hand from the lever to move towards the food reward at the end. The onset and offset time points of the isometric period are decided based on the vertical force being larger than a threshold (~0.11 N). On the bottom plot, the rectified-filtered versions of the neural signals show different patterns in each channel, indicating spatially selective recordings of the neural sources via different electrode contacts. Contrary to the force signals, the neural channels contain large components that are varying at fast rates.

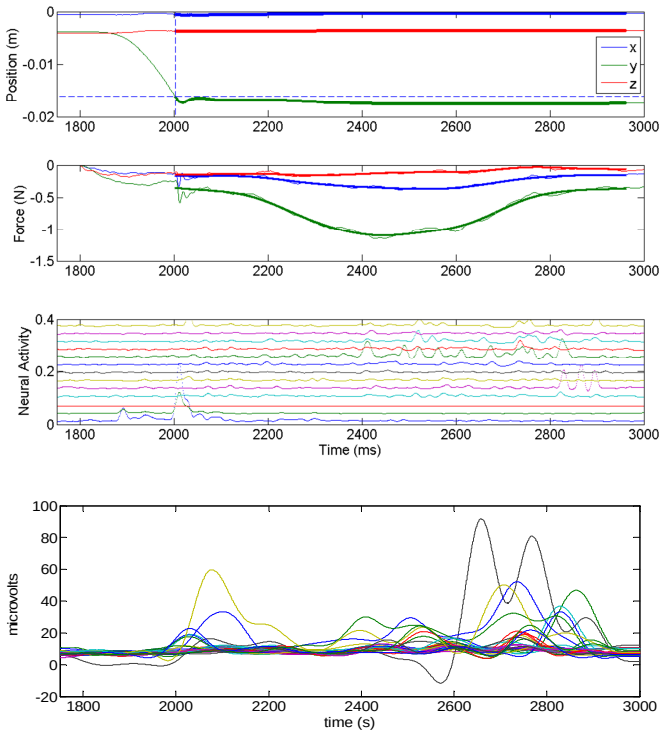

Figure 3.4 Plots of position (top) and force traces (middle) from a typical lever press trial. The isometric portion of the trial that was used in regression analysis is highlighted. A threshold force value of 0.11 N was used to mark the starting and ending points of the isometric region. The bottom plot shows the rectified averaged neural signals for 13 of the thirty channels in arbitrary scale as a sample. The two last figures show the same neural signals with two different filters.

3.2.1 Optimizing the Regression Coefficients

As mentioned above, the number of PCs was varied to search for the best force prediction in each session. Correlation and R-squared values increased (not monotonously but) steadily as additional PCs were included in the regression until a point of diminishing returns (vertical dash line in **Figure 3.5**). Adding more PCs over-fit the training set and yielded smaller correlation and R-squared values in the test set, which means that the set of PCs corresponding to the dashed line produced the best possible reconstruction. Furthermore, inclusion of additional trials into the set (e.g. compare the plots for 16 vs. 46 trials in **Figure 3.5**) improved the prediction. This further suggested that the reconstruction did not select features that over-fit the training data.

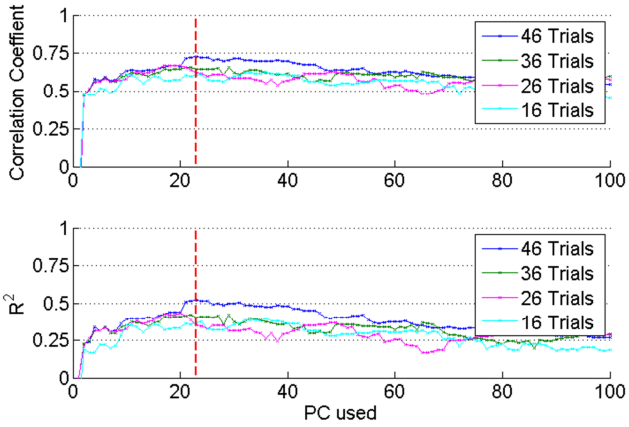

Figure 3.5 Searching for the optimum regression coefficients by increasing the number of PCs and the number of trials from the session included into the analysis. Top plot: correlation (R), bottom: R-squared values obtained by applying the regression coefficients to the test set. This procedure prevented over-fitting the data in the training set. PCs were sort in order of variance, increasing the size of training set gradually increase both the prediction effectiveness and number of PCs used.

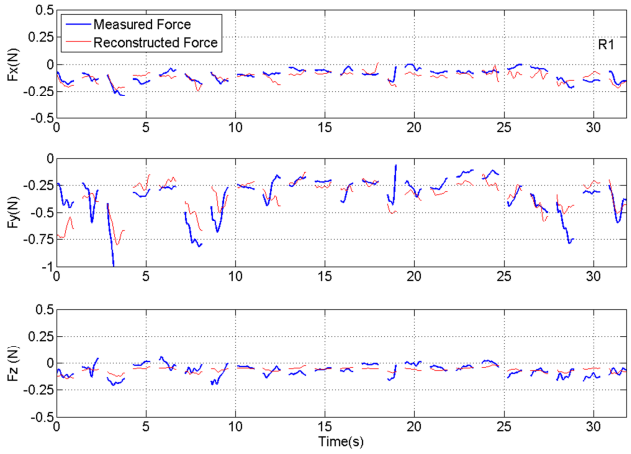

Figure 3.6 Plot of measured and reconstructed forces in all three directions in a set of test trials from one rat. Discontinuities in the plots separate the isometric force segments taken from different trials. Overall correlation and R-squared values are given in **Table 3.1**.

3.2.2 Reconstruction of Forelimb Forces

Forelimb forces in all three directions were reconstructed by applying the best coefficients to the test set (**Figure 3.6**). Prediction was more effective for the absolute magnitude (not shown) and the vertical force than the other two directions in this and other animals, as indicated by the R and R-squared measures. In general, the reconstruction algorithm was more successful in predicting the average force amplitude than the rapidly changing components of the forces in each trial (see Section 5.2.1 for a discussion about this). Coefficients of correlation between reconstructed and measured forces for individual trials (not shown) were not as high as the overall value for groups of trials in a training or test set. This is because the correlation coefficient for the entire test set accounts for the baseline changes from trial to trial but the correlation for an individual trial removes the baseline and only looks for the resemblance between phasic components of the predicted and actual force profiles within a trial. Thus, the R values

mostly represent the success in reconstructing the baseline level changes of the forces across multiple trials, although the phasic components are reproduced in some of the trials.

3.2.3 Frequency Contributions

Because the neural signals were separated into various frequency bands (**Figure 3.3**), it was possible to do back projection and determine the frequency components and the neural channels that were selected more often than others by the regression algorithm. The relative contributions of various neural channels and frequencies are plotted in **Figure 3.6** for R1. The middle bar plot in the bottom is the vertically averaged version of the map on top to investigate relative power contributions in different frequency bands to the y-force, with no attention paid to the channel number. The bar plots for the other two directions (X and Z) were produced from similar maps. It is interesting to note that lower frequencies contributed more to the predicted force in all three dimensions (see Section 5.2.2 for a discussion). There is a local maximum around 300 Hz in the X and Y axes. The small standard deviation bars suggest that the frequency contributions are relatively stable across multiple trials and somewhat similar in all three directions in this session. The analysis was retrospectively limited to frequencies below 425 Hz since percent contributions above this frequency were negligibly small. Components below 75Hz had to be disregarded due to movement artifacts.

3.2.4 Spatial Distribution of Neural Sources

The spatial organization of the neural channels (i.e. contacts) on the array could also be determined by back projection. Figure 3.8 illustrates the signal strengths (in all frequencies) by each contact on the array for all directions of force in Rat 1. Interestingly, certain contacts were selected much more frequently than others and these contacts are located mostly near the distal end of the array for all three directions of force. No single contact dominates as a single signal source and yet not all the contacts make a significant contribution either. The standard deviations (rings around contacts) are not very large, which suggest spatial stability of the neural sources that are selected by the algorithm across multiple trials in the same session (i.e. same day).

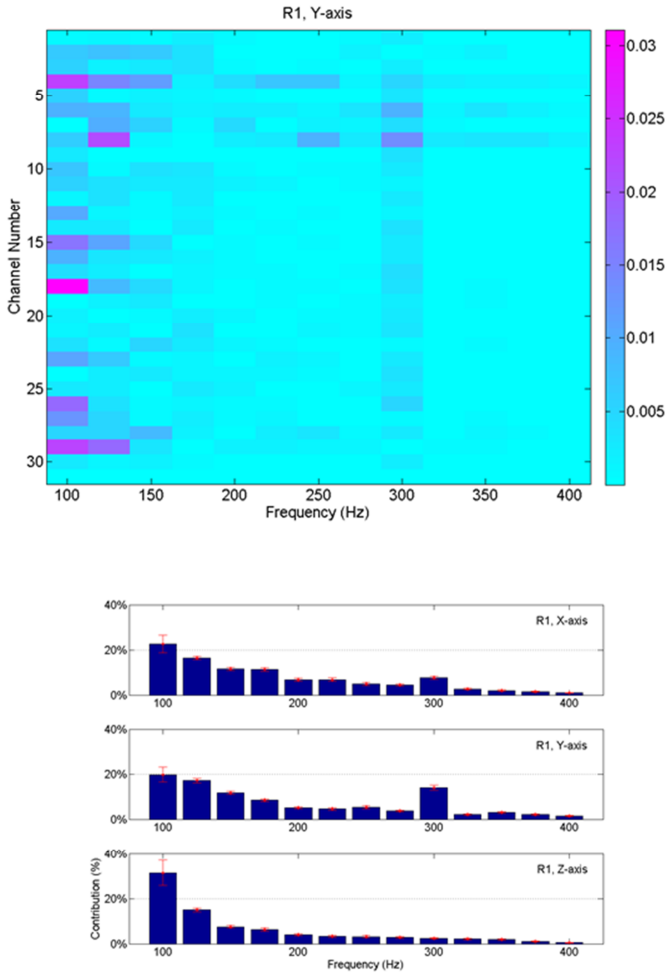

Figure 3.7 Average neural contributions with different frequency contents to the reconstructed forces in the trials shown in **Figure 3.6**. A: Contributions from the contacts of the array vs. the frequencies; this plot is for the vertical force only. Each small rectangle indicates the variance across multiple trials at the corresponding frequency by the corresponding contact multiplied by its regression coefficient. B: Contributions from all contacts are lumped together and the mean and standard deviations are shown as a function of frequency for all three directions of the force. Highest contributions come from lower end of the spectrum, although there is a local maximum around 300 Hz for X and Y forces.

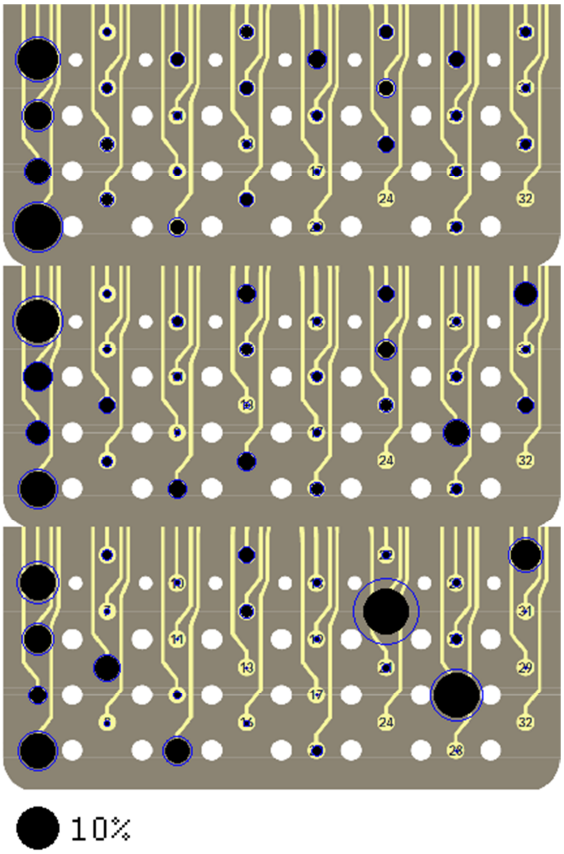

Figure 3.8 Signal contributions from individual neural channels superimposed on a map of the electrode array in Rat 1. Each array picture contains percent contributions for one direction of the forelimb force (X, Y, and Z, top to bottom). The sizes of the filled, black circles indicate average percent contributions across multiple trials and the rings around the circles show the standard deviations. The large black circle on the bottom represents a contribution of 10%. Contacts 24 and 32 were not recorded from.

3.2.5 Group Results

Force reconstruction plots (from the test set) in the remaining rats of this study (except that of **Figure 3.6**) are shown in Figure 3.9. Only the vertical forces are plotted for brevity. In each implant, the vertical force amplitudes were predicted by the algorithm with a positive correlation coefficient that is above 0.58. The duration of the isometric lever holding and the force profiles during were substantially different between trials. Moreover, each animal had somewhat different strategies of lever pressing behavior. Therefore, the force data profiles did not appear to be stereotypical and thereby allowing a large area of the parameter space to be visited.

The frequency band contributions to the vertical force predictions are shown in Figure 3.10 for all the animals. The mean and standard deviations are calculated across all the trials in the test sets. As in **Figure 3.10**, most of the signal power comes from the lower frequencies, except in R4 where there is a peak around 300 Hz. Again, the band limited signal contributions deviate from the mean only slightly across multiple trials in each animal.

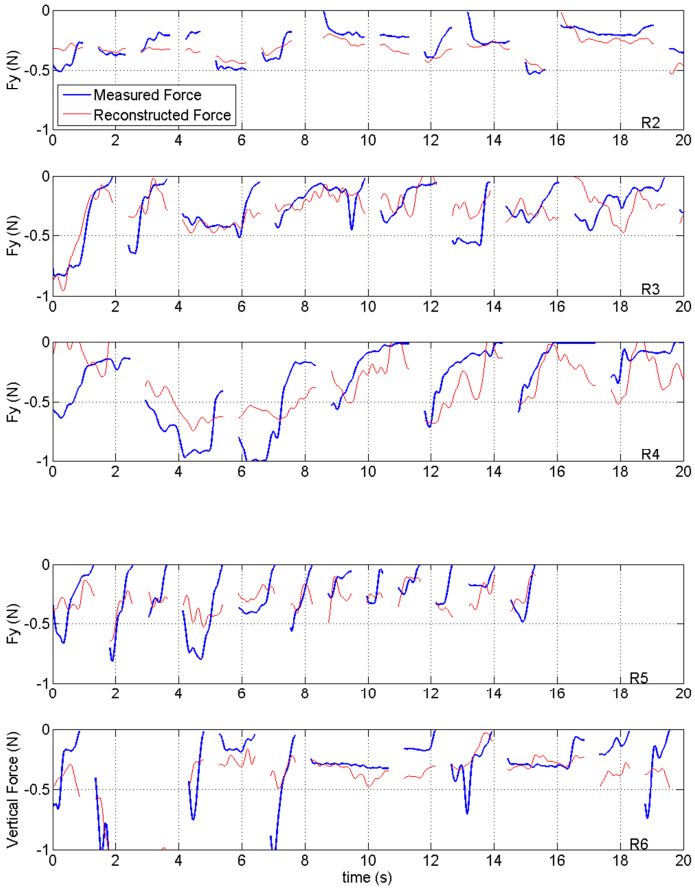

Figure 3.9 Plot of measured and reconstructed forces in the test sets from all rats of the study, except the one shown in **Figure 3.6**. Only the vertical forces are shown. Correlations and R-squared values are given in **Table 3.1**.

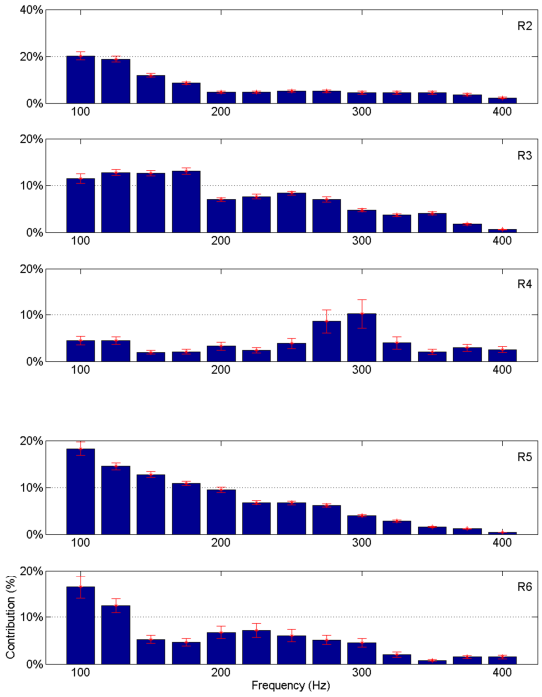

Figure 3.10 Percent neural contributions to the vertical force (Y) in different frequency bands, for all the rats in the study except the one already shown in **Figure 3.7**.

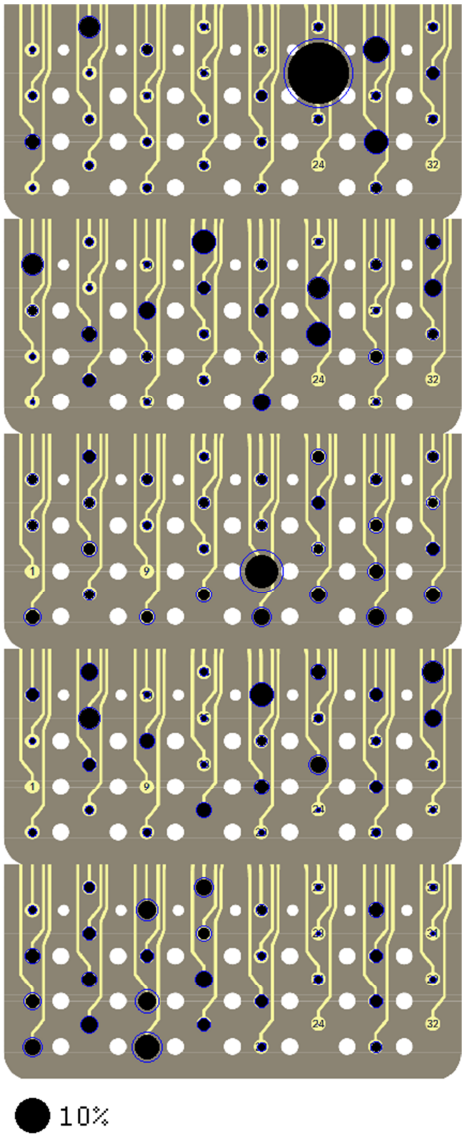

Figure 3.11 Signal contributions to the vertical force (Y) from individual neural channels superimposed on a map of the electrode array for the rats R2 through R6 (top to bottom). See **Figure 3.8** caption for further clarifications. Rarely does a single contact dominate the prediction, only in two cases contribution from a single contact was greater than 10%.

The spatial locations of the neural sources are depicted in **Figure 3.11** for the remaining rats of this study, excluding the one in **Figure 3.8**. Only the vertical force maps are shown for brevity. The fact that the standard deviations are small, particularly for the contacts with large percent contributions, increases the confidence level in the reproducibility of the neural source locations within the spinal cord. The map does not reveal a preference in the dorsoventral direction to point a certain depth where most neural sources controlling the forelimb muscles might be located in the spinal cord cross-section. That is, the plots do not support the presence of somatotopic organization in the corticospinal tract. The map looks completely different in each animal, as expected, since it is virtually impossible to implant the array in the same anatomical position even if there were not any differences between the animals. In general, the contributions distribute across many contacts and even the largest contributions do not go above 10%, with one exception in R2.

3.2.6 Statistics of Reconstruction

Group statistics are summarized in **Table 3.1** and

Table 3.2. The number of trials in the training and test sets are shown on the left most columns. The best correlation and R-squared values were obtained with R6, and the lowest coefficients with R5. Both measures were higher for the vertical force (Y) and the magnitude of the force vector (ABS) than that for the other two horizontal directions (X and Z) in all subjects. The vertical correlation varied between 0.58 and 0.77 with a mean±std of 0.66±0.07 (N=6). Similarly, the R-squared value for the vertical force changed between 0.33 and 0.59 with mean±std of 0.43±0.10 (N=6). The R-squared values are lower because it looks for an exact match between the actual and reconstructed forces, unlike the correlation coefficient which measures only the waveform similarity. Both measures for the ABS force were very close to that of the vertical force, presumably because the vertical force was the dominating component in the force vector. The last row in the table contains the mean values weighted by the number of trials in each test set. The weighted means are slightly higher because the largest test sets produced better predictions, especially in R5.

The statistics in **Table 3.2** are the mean correlations and R-squared values from the training sets that produced the coefficients. These numbers illustrate that the regression algorithm performed only slightly better in the training set than it did in the test set, and evidence showing that the regression was not an over fit to the data.

Table 3.1 Correlation (R) and R-Squared Statistics in the Test Sets From All the Rats of the Study

				TEST R				TEST R2			
RAT		TRAIN COUNT	TEST COUNT	X	Y	Z	ABS	X	Y	Z	ABS
1		46	23	0.65	0.73	0.52	0.72	0.35	0.52	0.26	0.52
2		38	18	0.60	0.64	0.53	0.64	0.36	0.39	0.24	0.38
3		34	18	0.56	0.62	0.51	0.60	0.30	0.36	0.25	0.35
4		51	26	0.59	0.67	0.43	0.66	0.35	0.44	0.17	0.42
5		22	12	0.24	0.58	0.33	0.53	0.05	0.33	0.10	0.28
6		81	39	0.69	0.77	0.49	0.78	0.46	0.59	0.22	0.60
Mean		45.33	22.67	0.56	0.67	0.47	0.66	0.31	0.44	0.21	0.43
STD		20.16	9.33	0.16	0.07	0.08	0.09	0.14	0.10	0.06	0.12
Weighted			0.60	0.69	0.48	0.68	0.35	0.47	0.21	0.46	0.60

Table 3.2 Overall Average Correlation (R) and R-Squared Statistics from All the Rats of The Study

				ALL R				ALL R2			
RAT			TOTAL COUNT	X	Y	Z	ABS	X	Y	Z	ABS
Mean			68.00	0.57	0.72	0.50	0.70	0.32	0.53	0.26	0.50
STD			29.47	0.13	0.10	0.09	0.10	0.14	0.14	0.09	0.15
Weighted				0.58	0.71	0.47	0.70	0.32	0.51	0.23	0.49

3.3 Discussion

3.3.1 Frequency Analysis

Time-Frequency analysis [57] was invaluable in separating the neural signals that are most relevant to the forearm forces. Short Time Fourier Transform allowed multiple time-varying signals to be generated from a single physical channel. A single physical electrode can carry information from different neural sources in different frequency bands and extraction of these sources into different channels was useful to improve the prediction. It is important to note that greater availability of signals required a larger training set. Additional trials were required to accurately estimate the extended set of coefficients.

The persistency of relative signal contributions to the force in various different frequency bands (Figures **Figure 3.7** and **Figure 3.10**) can be interpreted in different ways. This may be because the neural signals are composed of individual action potentials that have stereotypical shapes, which implies similar frequency components. However, the multi-unit neural signals usually occupy a frequency band starting around 300 Hz and reach up to a few kHz. The entire spectrum may have moved to lower frequencies in these recordings because of the small size spectra of the fibers in the rat CST. The fact that the frequency spectrum of the raw neural activity was reaching up to 1 kHz and even higher argues against this interpretation. Individual action potentials were observed to last 3-4 ms in the raw data. Although slow, the fundamental frequencies and harmonics should still be above 250Hz. The large contributions below 200 Hz may be interpreted as local field potentials. This raises the question if there is a contamination from the gray matter neurons into the recorded activity. However, the largest neural

activities are not recorded from the most ventral contacts in **Figure 3.11**, as one would expect if the array is too close to the gray matter in the dorsal column. Therefore, the most plausible explanation is that the low frequency components are the local field potentials arising within the white matter. Although the local field is a terminology that usually applies to the gray matter recordings, slow frequencies can theoretically be recorded within axon bundles if the neural spike frequencies are modulated as a function of time. If this is true, the descending activity in the CST must be varied by the cortical networks at rates in the high gamma band (60-90Hz) and higher frequencies. If indeed it is the local field potentials where the predictive power of the signals lie, the regression coefficients are expected to be stable over time once the chronic tissue response stabilizes to the electrode. Unlike the single spike recording technique, the local field potentials should be immune to micro motions of the implanted electrode.

3.3.2 Factors on Regression Success

Compared to brain-computer interfaces where single spike activities are used to predict the forelimb or arm kinematics, the spinal method should be able to access signal with much richer volitional content. Nonetheless, it may still not be possible to collect all the forelimb related activity from the CST because of the limited recording range of the electrode array. The dorsoventral extent of the electrode is approximately 300 µm and it matches the size of the CST in the rat. However, majority of the fibers are smaller than 3.7µm in the CST [58] and the number of recording contacts in the array is too small compared to the number of neural sources if majority of axons become active at any time instant. This issue of under sampling the available neural sources can be resolved to a large extent with much denser arrays and smaller contacts.

Force prediction could also be limited by the fact that the RST activity was not accessed in this study. The RST plays an important role in voluntary movements both in rodents and primates [5, 59, 60]. The RST is also known to take over the function of an injured CST [61]. A second array implanted in the RST can demonstrate the predictive power of this tract in comparison to the CST in different behavioral contexts in future experiments.

Accounting for the neuromuscular delay had negligible effects on the success of reconstructions. This may be explained by the small propagation delays. The myelinated descending fibers reach up to velocities ~19 m/s and the mean velocity is about 11.4 m/s [22], where the latter may be an overestimation in the cited study because of the tendency of microelectrodes to record mostly from larger and hence faster fibers. Nevertheless, because the distance to the muscle is only in the order of centimeters, most of the delay can be attributed to muscle activation. The delay from the stimulation of cervical gray matter to the forelimb force initiation was less than 50ms (unpublished results) in anesthetized rats. Because the forelimb forces did not contain very high frequencies, accounting for the neuro-muscular delay did not have a substantial effect on regression results.

3.3.3 Recording Electrodes

Two other types of electrodes were tested previously and the performance of flexible electrode arrays was deemed superior to both for this application. Utah type penetrating electrodes can generate severe neural damage in small animals due to their rigid substrate not conforming around the spinal cord [62]. Flexible electrode array also offered an

additional benefit of recording from multiple sites in the same sagittal plane. The well-defined contact positions allowed a more uniform sampling of the CST activity in the mid-sagittal plane. Single wire electrodes had a tendency to disintegrate [28] faster than the flexible electrode arrays even when wires were bundled within a silicone tube. Furthermore, the relative positions of wire electrodes were very difficult to control during implantation.

3.4 Conclusions

This study demonstrated that the forelimb isometric forces can be predicted using the corticospinal tract activity recorded from the rat cervical spinal cord. The flexible MEAs may be a good choice to achieve a mechanically stable neural interface in the spinal cord. These results support the supposition that spinal cord-computer interfaces can eventually be built for subjects with spinal cord injury to operate manipulators with relatively little training, provided that other issues such as tissue reaction and reliability of electrical interconnects can be overcome.

CHAPTER 4

EVIDENCE OF POSITIONAL DEPENDENCE IN DESCENDING FORELIMB SIGNALS IN THE RAT SPINAL CORD

4.1 Methods

4.1.1 Behavioral Training and Surgical Procedure

The behavioral training and Surgical Procedure is identical to those conducted for the study described in the previous chapter. Please consult Sections 2.1.7 , 3.1.1 and 3.1.2 for details for these procedures.

4.1.2 Apparatus

A time varying force field (See Section 2.1.2) was designed with the following properties: Before T1 the lever is restored to its up position by a 20 ms pulse of 2 N and held in position by a servomotor-controlled spring-damper with setpoint, Y_0= 0 mm, and spring constant, K=256 N/m, and damping constant, B=16.384 N/(m/s). The spring is deleted after one second and replaced with damper only, B=4.096N/(m/s). With no applied force, the lever remains at Y_0. When animal places its forearm on the lever (T2), it is displaced downward. When the lever reaches the specified arrest height, Y_f shown at T2, a new one-sided spring-damper is initiated with its setpoint at Y_f, with high stiffness and damping, K=2048 N/m and 16.384N/(m/s), to generate a crisp arrest of downward movement. Thus the spring is effective only preventing movement past Y_f and does not affect movement above Y_f, thus creating the isometric period of interest in this study.

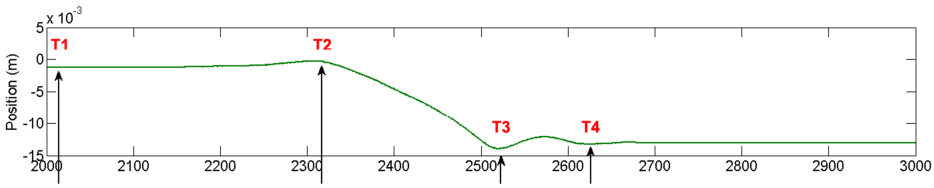

Figure 4.1 time course of the position in the control trial.

4.1.3 Data Collection

The method of data collection in this study was identical to that of the previous study. Please consult Sections 2.1.3 and 3.1.3 for a review of the data collection method.

4.1.4 Experimental Procedure

Experiments were designed to record isometric neural and force data at various positions in order to determine whether mapping from neural data to isometric force at one location completely predict isometric forces from neural signal at another. Testing occurred on multiple days allowing for 90-100 trials in which the animal pushed the lever and received food until its appetite was satisfied. While the animals were all trained to push to a fixed arrest height (e.g., 15 mm) only 60% of the test trials were terminated at the trained height. Randomly interspersed among the remaining 40% of the trials in which the arrest was made (unexpectedly to the animal) at a different height. Two thirds of the trials arrested at training height were used as the training set for determining the function that maps neural signal to predicted force. Remaining trials arrested at training height were used as a test set to verify the accuracy of the mapping weights. The trials terminated at different heights were used as a second test set to examine the ability of the mapping function to predict forces of trials arrested at heights other than the trained arrest position.

4.1.5 Estimating Force from Neural Signals during Isometric Phase

The methods used to estimate mapping from neural signal to isometric position was identical to those used in the previous study. Please consult Sections 2.1.9, 3.1.4 and 3.1.5 for details.

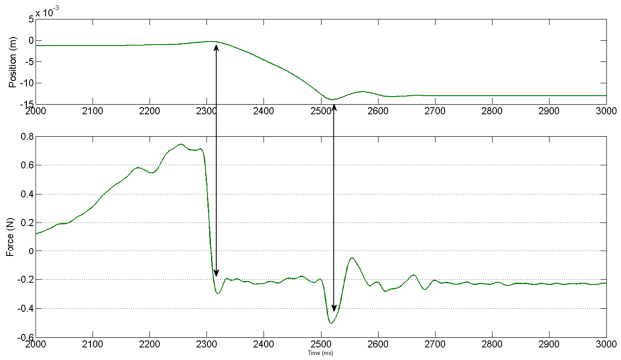

Figure 4.2 Control Trial. A weight was placed on the lever, which was held up by a string. The string was cut and lever fell to target position. The force sensor measured a near constant level of force during the fall.

4.1.6 Overview of Analysis Algorithm

According to Equilibrium Point Hypothesis (EPH), a given Virtual Trajectory (VT) produces parallel forces trajectory for different isometric levels. The difference between these forces depends only on the distances between the isometric locations.

Because isometric coefficients were derived at some fixed isometric height and do not contain coefficients for position, the predicted force for a trial is the force that would be generated by the same VT at the height were the coefficients were derived, plus an AC noise component. Ideally the predicted and measured force should be parallel.

Under fixed isometric conditions the intent and force are one of the same; therefore effectiveness of prediction (reconstruction) is the same as effectiveness of estimating the intent.

Therefore, the measured and estimated force can considered as force trajectories generated by the same VT. The relationship between position and position-dependent force can be derived by plotting their mean difference against position (For a mathematical analysis, see Section 4.3.2). A positive slope indicates instability (or negative spring constant): movement in one direction lead to increasing force in the same direction. A negative slope indicate stability (or positive spring constant): movements in one direction lead to increasing restoring force in the opposite direction.

4.1.7 Static Error Analysis

Sessions containing mixed trials were carried out. The haptic system was programmed to stop 60% the trials at a predetermined position. The remaining trials were stop at random positions. Neural weight coefficients for isometric force were estimated using trials

halted at the fixed position. The coefficients were then used to predict isometric forces for remaining trials.

Means and standard deviations of prediction error (Measured Force - Prediction) were calculated for each trial. Trials with very large error mean or deviations (>0.2N) were considered failed predictions and discarded. Trials with large error mean or deviations overlapped strongly with trials with aberrant movement profiles. (e.g., the animal pressed the lever with both arms or rested its head on the lever). Trials stopped at predetermined position and were used to estimate the mapping was also excluded from the calculation.

An optimization was performed to determine the height of stability transition. At this height the rat switches from a stable bipedal posture to an unstable quadruped one (see Section 4.3.4). Therefore this point is at the maximum of the theoretical force-position relationship. The optimization finds a height that minimizes correlation between stop position and mean error of all trials stopped above it. Trials were then grouped depending whether they were stopped above or below this height and the slope between mean errors and positions were calculated for each group using robust fit.

A moving Gaussian window with sigma of 1mm was applied to the signal produce a non-parametric estimate of relationship between mean error and position. This estimate is displayed in green on the result figures.

4.1.8 Controls for Static Error Analysis

To test whether relationships between prediction error and position is a consequence of spinal signals, control were performed for each session. Predictions were calculated using

zero mapping weights instead of regressed mapping weights (**Figure 4.4**). Mean errors were centered by subtracting their median. The reminder of the error analysis was performed as described in the previous section.

4.2 Results

Four animals from the last study were used for this study. Dropping rat 1 and 3 from **Table 3.1** produced result below. Rat 1 did not participate in this experiment because it performed no arrested trials, Rat 3 did not participate because its posture was always unstable.

Table 3.1 and **Table 3.2** shows the R and R2 values for the test set containing trials at the originally trained stopping height. The mean R (.66) and R2 (.43) values for the Y direction are the highest among the Cartesian directions. This is to be expected as the trained activity was to move the lever in the Y direction. This shows a strong prediction of forces from neural signal.

Table 4.1 Table of R and R2 for Test Set with Varying Arrest Heights

RAT	Y R	Y R^2	R Reg. Halt	R^2 Reg. Halt	Delta R	Delta R^2
2	0.635	0.389	0.511	0.243	-0.124	-0.146
4	0.672	0.438	0.609	0.349	-0.063	-0.089
5	0.58	0.332	0.251	-0.178	-0.329	-0.511
6	0.773	0.591	0.382	0.076	-0.391	-0.514
Mean	0.665	0.438	0.438	0.123	-0.227	-0.315
STD	0.081	0.111	0.155	0.23	0.074	0.119
Weighted	0.695	0.478	0.495	0.206	-0.2	-0.273

4.2.1 Analysis of Static Errors

Analysis of the prediction error (measured force – predicted force) among the test trials with differing arrest heights for each animal showed that this error was not a constant function of position. **Figure 4.3** shows the mean error for each termination height in the training and test sets for rat 2. The black shows the mean error of all trials terminated at the original trained height. The average of all error was centered near 0. The blue shows that the mean error of trials arrested before the trained height has a negative slope. In, **Figure 4.5** a Red line shows a positive slope for mean error of trials terminated beyond the trained slope. Plot so mean error for other animals have a very similar appearance. Statistically speaking, rats exhibit a spring constant of 21.4N/m (± 9.3N/m) above 15mm. below this height there is no reliable dependence -7N/m(± 15.1N/m).

There appear to be two major regimes in the force/position relationship of all rats. If the lever was halted above 15mm, the slope of prediction error is negative, suggesting a force that acts in opposition to displacement. If the lever was halted below 15mm, the slope of the error is positive, suggesting force acting in direction of displacement.

The first two rats were rewarded when they reached 14mm during training and the remaining rats were rewarded at 18mm. Stability at high isometric position and instability at low isometric positions were observed in all animals, regardless of their training targets.

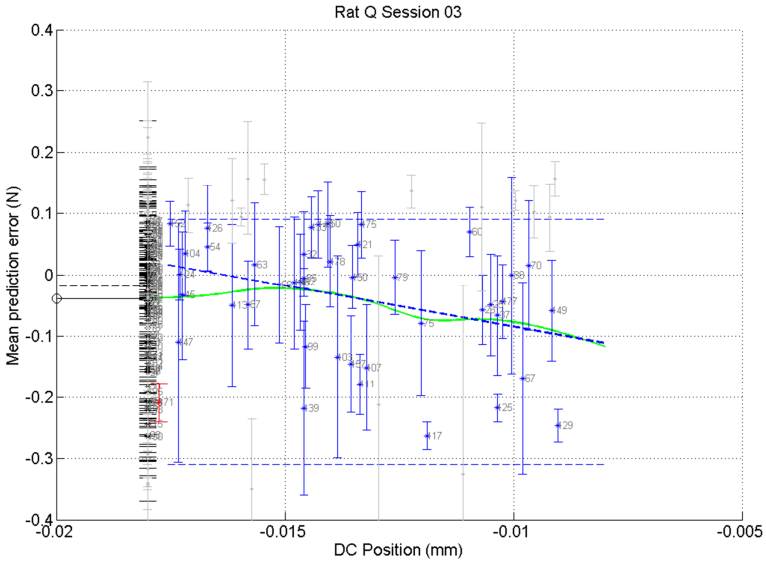

Figure 4.3 Static Error Analysis for Rat 6 (last row in table 2) Blue: Trials in the stable region with robust regression estimate. Red: trials in the unstable region. Black: Trials used to generate isometric coefficients for neural prediction. Grey: Ignored trials Error Bars indicate the variation of prediction error within individual trials. Green line: Gaussian estimate of Force/Position relationship for the session.

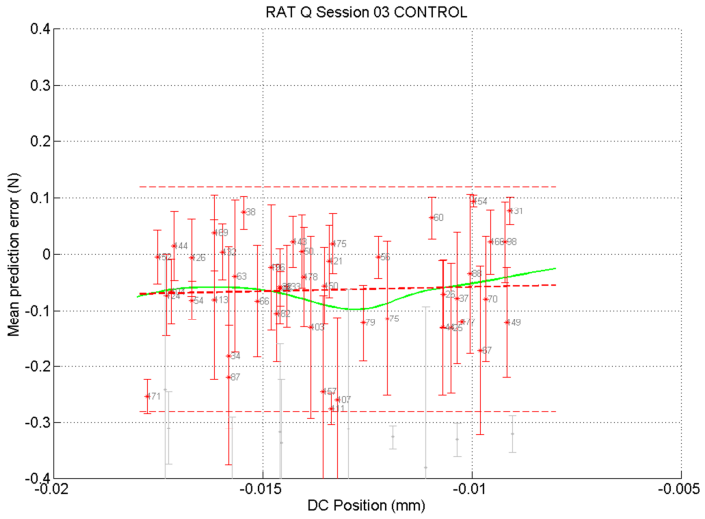

Figure 4.4 Control for the session in **Figure 4.3** All isometric coefficients except for the Non-neural dependent DC term was set to zero. When prediction coefficients were set to zero, the same analysis indicate no relationship between force and position (K= 0.10143 N/m, p=0.62).

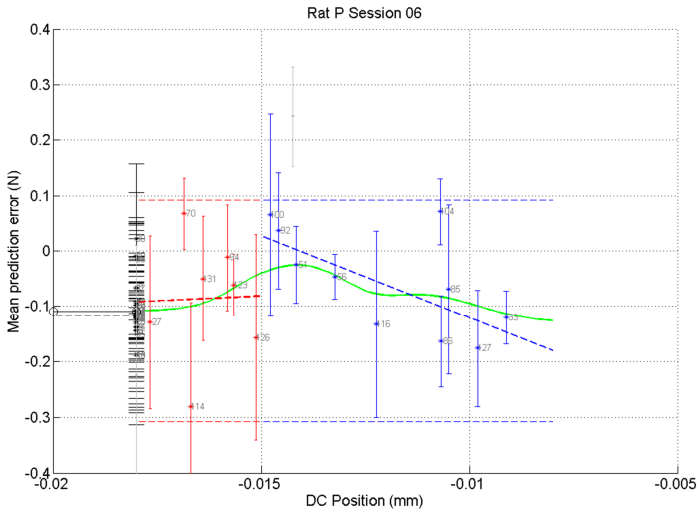

Figure 4.5 Force/Position analysis for Rat 5, second to last row.

Table 4.2 Overall Statistics Of Force Vs. Position: Slope Stable: Blue, Slope Unstable: Red.

STAB: Stable, UNST: Unstable, H. TRANS: Transition height

RAT	HALT CNT	STAB COUNT	SLOPE STAB	P STAB	UNST COUNT	SLOPE UNST	P UNST	H. TRANS	CTRL CNT	SLOPE CTRL	P CTRL
2	43	23	-29.702	0.081	20	23.92	0.1	-0.013	28	-3.033	0.86
4	72	39	-13.374	0.09	33	-5.475	0.766	-0.015	15	-40.023	0.18
5	17	10	-29.348	0.04	7	3.35	0.961	-0.015	21	9.795	0.313
6	42	42	-13.318	0.032	0			-0.018	47	1.484	0.779
Mean	44	29	-21.435	0.061	15	7.265	0.609	-0.015	28	-7.944	0.533
STD	22	15	9.342	0.029	15	15.084	0.452	0.002	14	22.036	0.337
Weighted			-18.048	0.062		5.353	0.567	-0.015		-3.692	0.63

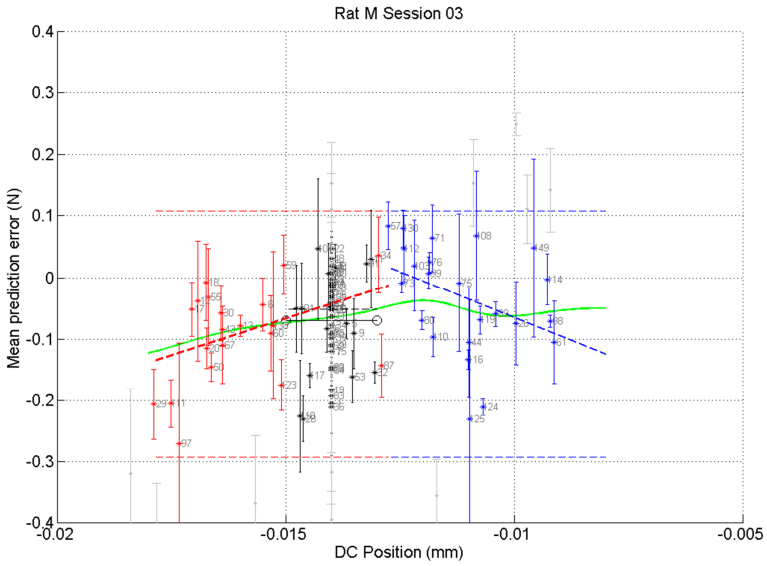

Figure 4.6 Force/Position analysis for Rat 2, first row in the statistic.

4.2.2 Examination of Non-Passive Lever Pushes With Trained And Arrested Terminations

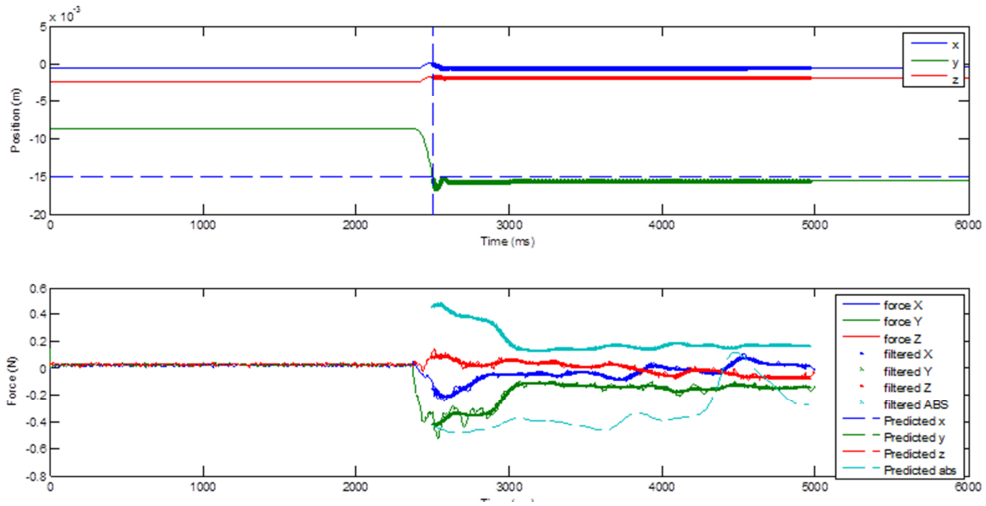

Figure 4.7 Arrest at 15mm.

Kinematic and kinetic examples of a reach to the lever was shown here (i.e. no force on the lever before push is initiated.) In **Figure 4.7**, the arrest is at 15mm and in **Figure 4.8** it is at 12mm. The EPH would predict that if the descending signal were the trajectory of an attractor, the same attractor would be applied in both cases due to training. The arrest at 12 mm would produce a larger distance between the arrested position and the attractor, resulting in a larger force immediately after the arrest. Such results have been seen in human studies in which a limb is perturbed by a manipulandum (usually a haptic interface). This pattern is seen in a subset of the rat trials typified by this example . A force of -.35 N is found after the end of the dynamic period in the 15 mm arrest and a force of -.67 N is measures when the arrest is at 12 mm. As these represent one of the four rat strategies, further analysis of this specific strategy is anticipated.

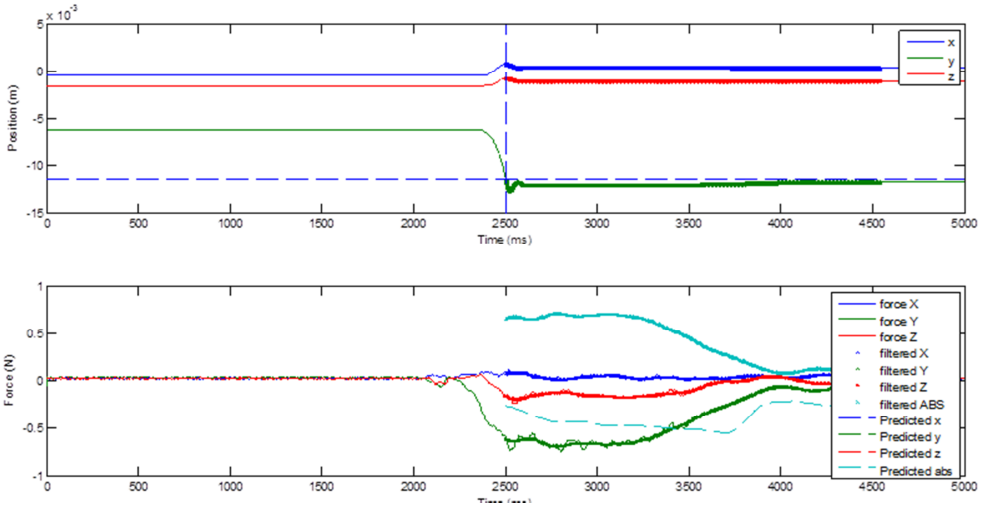

Figure 4.8 Arrest at 12mm.

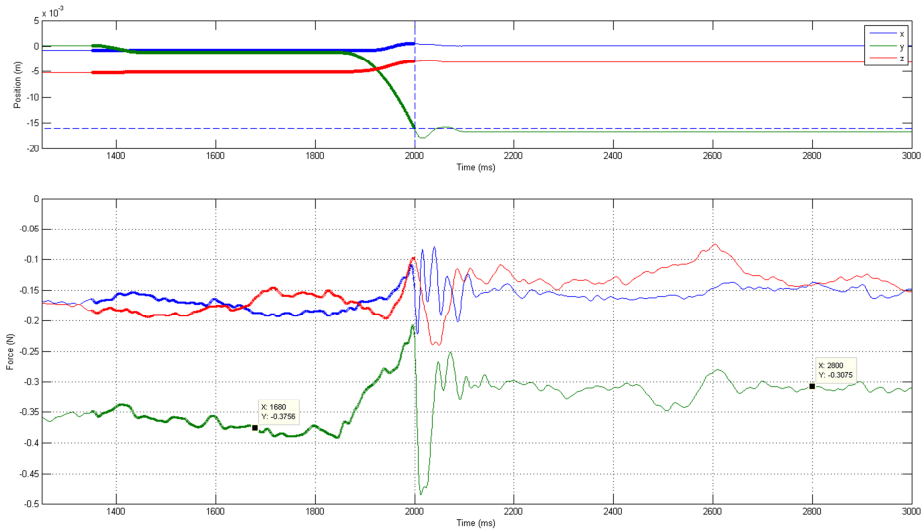

Figure 4.9 Example of isotonic force control. Sudden movement of lever between 1850 and 2000ms resulted in force changes in the opposite direction. The isometric force was maintained between .3 and .4 newton before and after the movement, regardless of position.

4.2.3 Isotonic Trials

A significant number of trials were observed where the rat exerted a nearly constant level of force regardless of position, as long as no rapid movements are taking place. (**Figure 4.9** shows a typical trial of this kind). However, in these trials rapid changes of position cause force to change in the opposite direction.

4.3 Discussion

4.3.1 Choice in Segments of Interest

There are several reasons for this study to focus on the isometric force after the lever press rather than the lever press itself. First, the estimation of mapping from neural signal to force could only be carried out using only isometric data collected at the same height, because the mapping did not contain terms that account for position. Since it's possible that force depend on position, estimating mapping using data collected under non-isometric conditions or from different positions introduces an error in the mapping. Secondly, study of isometric forces eliminates the need to account for dynamics. There is no need to account for the relationship between velocity and force under isometric conditions, this make easier to estimate the neural-force mapping.

Another reason for studying only the isometric data is observation of passive lever presses. A number of trials were similar to the one below. The animal distributed its weight onto the lever, so it fell each time it was reinitialized without additional effort from the rat. In this situation, the relevant command signal to shift the weight occurred before the lever press, and no signal relevant to weight generation is present before onset of the isometric condition. Analyzing neural signal during the lever press when the animal is passive reduces signal to noise ratio.

Even when an animal is pressing the lever passively, it must redistribute its weight in order to handle food pellet, therefore analysis of isometric activity always contain signals relevant to the force generated.

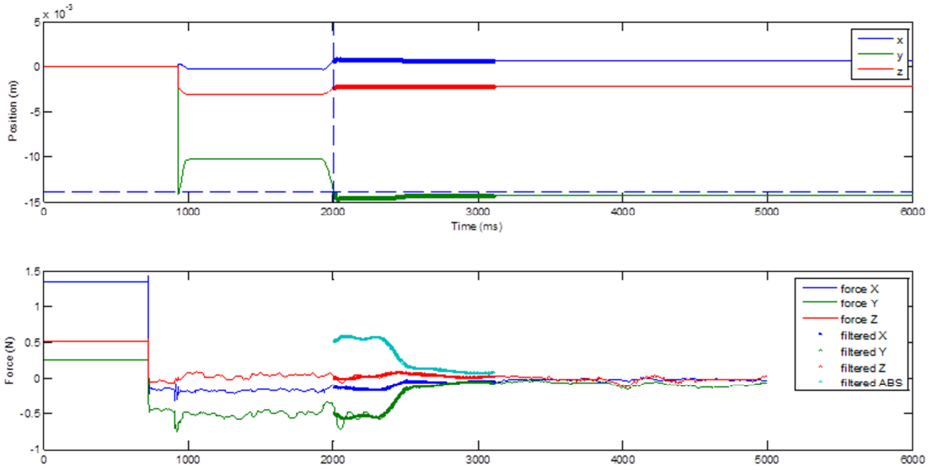

Figure 4.10 an apparently passive trial.

4.3.2 Analysis of Neural Code under Isometric Conditions

Power Spectral Density weight coefficients were estimated using isometric segments of a series of trials. These weights have different implications according to different theories.

Under the Equilibrium Point Hypothesis, positional feedback generates forces according to a descending reference signal. Forces measured under isometric conditions are proportional to the reference trajectory. Therefore the force estimation under this condition can be also considered as estimation of the reference trajectory.

$$f(\vec{N}) + \tilde{e} = F(t) = k(x_0(t) - X) \quad (4.1)$$

$$\vec{N}(t) = [n_1(t) \quad n_1(t) \quad ...]$$

$$f(\vec{N}) = \langle \vec{w} \cdot \vec{N} \rangle$$

Where $f(\vec{N})$ is force estimation, $\vec{N}(t)$ is vector of neural Power Spectral Densities. $\tilde{e}$ is the estimation error, a random variable centered on 0. $F(t)$ is measured force. k is a positive spring constant. $x_0(t)$ is the theoretical reference position and X is the fixed position for the isometric segment. For simplicity force is estimated as a linear combination of neural PSD without rectification.

According to Inverse Dynamic hypothesis, local feedbacks are disabled when an animal carries out a voluntary action. Therefore, neural signal encodes pre-calculated forces. In the other words:

$$F(t) = f(\vec{N}) + \tilde{e} \quad (4.2)$$

Hold true for all voluntary forces, including those produced under isometric conditions.

4.3.3 Prediction Error Analysis

If local positional feedback exists below the level of recording, measured force is a function of both neural input and current position. Formally

$$F(t) = k\big(x_0(t) - x(t)\big) \tag{4.3}$$

Therefore the prediction error should be a decreasing function of position.

$$F(t) - f\big(\vec{N}\big) = (kX + \tilde{e}) - kx(t) \tag{4.4}$$

If local positional feedback does not exist, no relationship between prediction error and position can expected.

$$F(t) - f\big(\vec{N}\big) = \tilde{e} \tag{4.5}$$

4.3.4 Stability Change

Rats also exhibit unstable behavior (K=-58N/m± 45.6N/m) when the lever was sufficiently low. This was likely caused by transition to Quadruped postures. Redistributions of weight caused by this change can account for the instability at low isometric positions. This suggests that the animals were capable of planning postures that were unstable without external support.

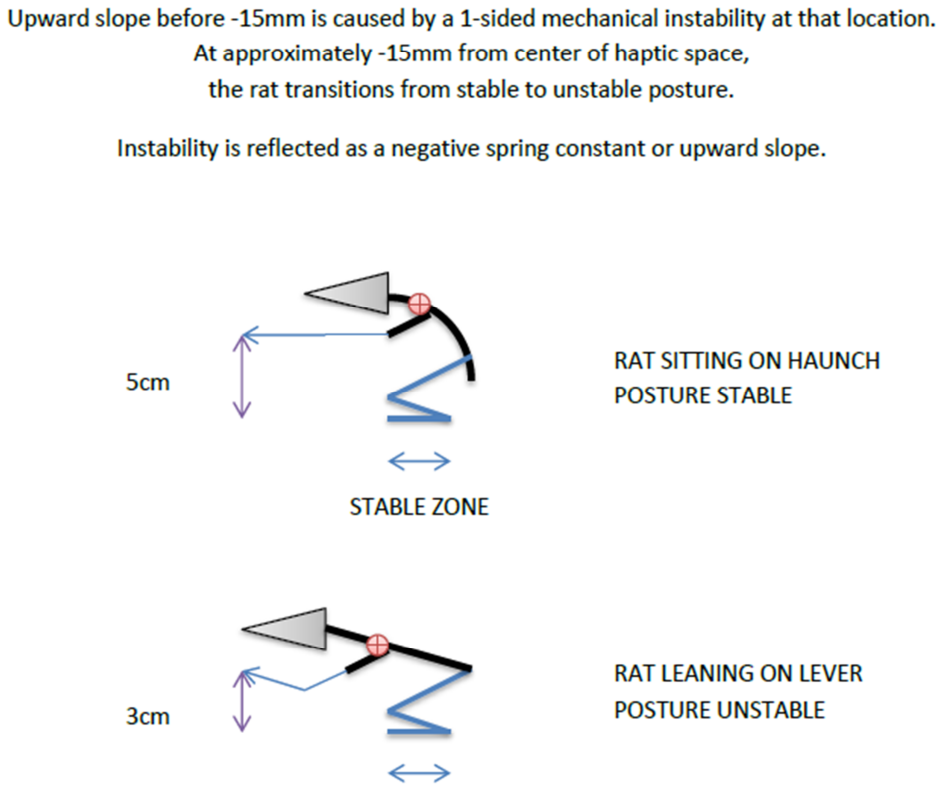

Figure 4.11 Illustration of postures in the stable (top) and the unstable (bottom) regime.

4.3.5 Evidence of Spinal Feedback

Rats respond to unexpected rapid forward movement of its paw with decreasing force. This is consistent with behavior of human subjects in loading experiments and is explained by equilibrium control.

Results from analyzing forces predicted from neural signals (**Table 4.2**) suggest that the neuromuscular system at the spinal level and below can exhibit spring-like behavior under isometric conditions. The lower the position, the more likely it is for the neural force trajectory to deviate from measured force trajectory in the same direction. The prediction error is expected to be centered on zero in absence of feedback regardless of position.

4.3.6 Close Loop Control of Force

It is reasonable to assert that well trained rats are aware of minimum forces required to drive the lever. Therefore, given enough time, such an animal would adjust its postures to produce a near constant level of force. This is observed in a number of trials.

If control of force requires the involvement of cortical or cerebellar systems, rapid changes in position would still result in change in change of force in the other direction until the animal adjusted its command signal to compensate. This is consistent with the observation.

Conscious modifications to posture can also be observed in the instability. The animals were capable of planning postures that would be unstable in the absence of the lever. A different command signal would be required for a similar posture that is stable without the lever. This implies that animals were able to encode posture that differs only by force output. The observation of both position dependent force and isotonic close loop control suggest the coexistence of internal models and spinal feedback.

4.3.7 Towards A Unified Theory of Motor Planning

Efference copies and (forward and inverse) internal dynamic models can coexist with spinal feedback. There are no irreconcilable conflicts between mechanisms behind Equilibrium Trajectory and Inverse Dynamic Control. Therefore evidence for local feedbacks should not be considered evidence against inverse dynamic model.

It is more probable that inverse dynamics and equilibrium control are models of systems that works in conjunction to deliver controlled movements. Spinal feedback stabilizes posture and movements against unexpected perturbations while internal models preemptively correct errors that can be anticipated and allow trajectories to be refined through motor learning.

The following figure presents simplified schematics of a possible unified control model. The coupled forward/ inverse internal dynamic model is shown on the left side of the dash dot line. The internal models combine desired force and position trajectories into a reference trajectory.

This trajectory descends to the spinal circuits on the right side of the dash dot line as gains of synergistic groups of muscles. Spinal feedback allows each synergy to define a static attractor or limit circle in the three-dimensional space. Altering the relative gains of multiple synergies defines the trajectory of a moving attractor in the same space. Proprioception is also returned to the brain as parametric feedback for tuning the internal models.

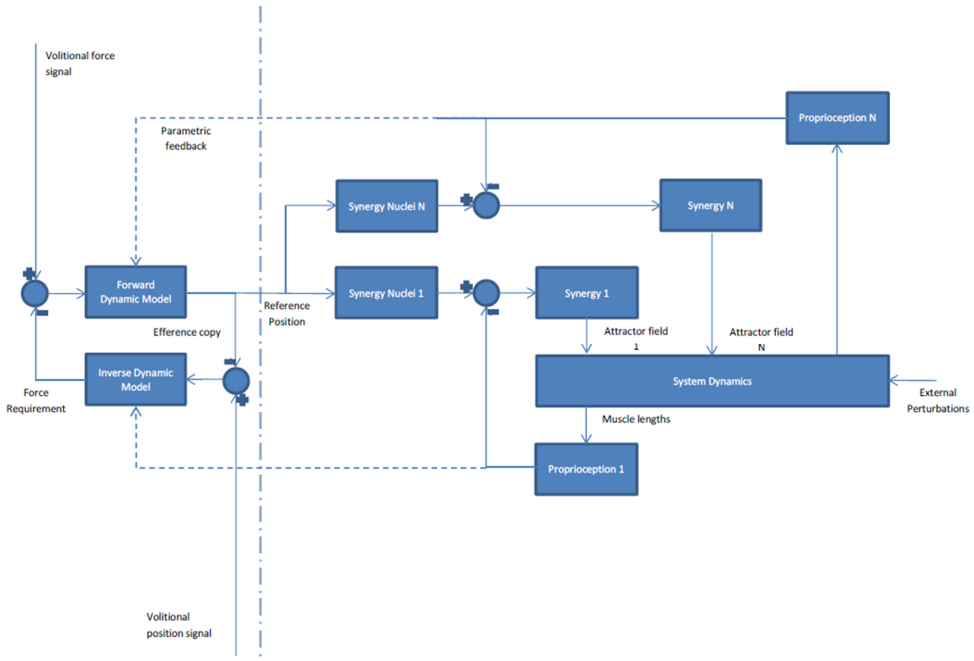

Figure 4.12 simplified schematics of unified control.

4.4 Conclusions

Inherent stabilities of rats during lever pressing tasks suggested that positional feedback exists at the spinal level. This is consistent with a descending reference position. Observed isotonic behaviors suggest that force may be controlled by modification to the reference trajectory in the presence of cortical and/or cerebellar feedbacks.

4.4.1 Implication in Design of Neural Prosthetics

Robotic actuators under control of Brain computer Interface or Spinal cord Computer Interfaces should emulate positional feedback of circuits they replaces. This feedback is vital in any application where stability is important. Furthermore, for such devices to perform fast movements, velocity feedbacks should be implemented. [63]

In addition, High performance robotic actuator controlled by neural signals should contain inverse dynamic model of the limb they intend to replace. Because the descending reference signal can contain both intended position and force, an inverse dynamic model is required to separate them.

CHAPTER 5

DISCUSSION

5.1 Overall Conclusions

This project concludes that a linear model is sufficient to predict isometric force from only corticospinal tract signals. In practical terms this means Spinal Cord Computer Interfaces (SCCI) that require relatively little training to operate are possible, providing the reliability of electrodes can be improved.

The project also determined that positional feedbacks are performed by spinal cord circuits and the descending control signals to the spinal cord are likely referential positions. The practical implication of this observation is that actuators driven by SCCI can benefit from positional feedback and inverse dynamic model of the limbs it intend to replace.

5.2 Theoretical Discussion and Speculations

5.2.1 Reconstruction of DC Force versus Fast Force Changes

The method described in chapter 3 is much better at reconstructing slow changes in the force than fast changing details of the force. Reconstructions were attempted with multiple different delays in order to determine the cause. Reconstructions were possible with delay up to 50ms. It stands to reason that different fibers in spinal cord have different conduction velocities. It may be possible to predict rapidly changing forces by estimating delay for each signal.

5.2.2 Possible Sources of Signals at Various Frequency Bands

Figure 3.10 suggest that neural signal come from two major sources, low frequency signal below 200Hz and high frequency signal below 200Hz. It is possible the low frequency signal arose from post synaptic activity in the nearby grey matter while the high frequency signal were result of activity of descending tract.

5.2.3 Speculation on the Coordinate System Of Voluntary Movements

It's unlikely the control signal to the spinal cord is encoded in Cartesian coordinates because it's possible maintain different elbow angle while holding the hand in the same position and orientation. This implies that descending command signal must encode movements in some abstract postural space.

Bizzi et al. has suggested a basis of this space in a recent paper [50]. According to that publication, muscles are controlled in groups, and together their activity defines an

attractor: either a point attractor or a limit circle. Movements were then constructed from these attractors.

5.2.4 Speculation on Parallel and Serial Feedback / Feed Forward Connections

The evidence presented by this project does not eliminate the possibility of parallel feedback/feed forward systems. **Figure 4.12** suggests the internal models are in series with the spinal feedback. It's possible for them to exist in parallel. It's possible that some lower motor neurons do not receive proprioceptive feedback and act as a feed forward "transient" controller.

This scheme was proposed by Alvarez et al [64] for the ocular motor system. It is possible this architecture also exist in other parts of neuromuscular system considering the existence of myriad of descending tracts. At the present there is no evidence pointing to type of architecture or the other.

5.3 Future Directions

While the thesis project has completed all of its objectives, a number of possible improvements have been realized during the investigation. A brief discussion should be dedicated to them for completion of this thesis.

5.3.1 EMG Analysis

Simultaneous EMG recording scan be used to explore the coordinate system of command signals. By predicting activities of muscles or groups of muscles, and comparing the result with prediction of overall force, it will be possible to study if the descending command is in muscle, joint or spacial coordinates.

5.3.2 Recording from Grey Matter and RST

Grey matter contains signal of interest. It was recognized that power of low frequency signals (60-100Hz) recorded by an electrode unintentionally placed in the grey matter could be used to predict force. Similarly previous work had shown that signals from Rubospinal tract can be used to prediction of joint angles.

Due to anatomical landmarks, reproducible recording from grey matter and RST is difficult. Final location of the implant can only be determined by histology. Therefore a large number of repetitions is required. Investigations into these areas are likely to yield useful result if additional resources can be directed to it.

5.3.3 Staging

The ultimate validation of SCI will be direct control of external actuators using neural signals. The DAQ system already performs FFT of neural signals. It's possible to compute an animal's intended position in real time after a transformation matrix is calculated from neural signals and force recorded at two positions.

Rats will undergo gradual training process where the Lever becomes increasingly controlled by neural signals. An attractor field will be placed at the computed target position. The strength of the attractor will increase gradually.

Unlike cortical signals, there is no difference between intent and command in the spinal cord - a spinal signal will generate force. This means that rat will continue to press the lever physically, but this force will move the lever, but the neural intention of them will. The effectiveness of neural control can be measured by the force exerted on the lever. In the ideal case, the lever should measure only gravitational forces.

5.3.4 Horizontal Movements

The transition from bipedal to quadruple postures interferes with analysis of stability of spring-like neuromuscular system. The study can be improved if rats can be trained to move the lever horizontally for a food reward.

The rat could be trained in the vertical lever press first. Then the force field that restores the horizontal position could be gradually rotated so that the path of resistance will become horizontal over time. Alternatively the fields that restores horizontal position should be disabled and the animal will be required horizontally displace the lever for increasing large distances. The neuromuscular system is expected to be stable for the entire range of horizontal motion.

5.3.5 Nonlinear Estimation Techniques

Difficulty in prediction of high frequency moment-to-moment change could be caused by variation in transmission speed of neural signal. Because time delay is a non-linear operation, it may be accounted using nonlinear models such as Volterra functional expansion or neural networks. These models can be estimated using well established techniques such as Laguerre basis function and error propagation.

However nonlinear models present additional technical problems. Neural networks are opaque to interpretations and volterra kernel further expands dimensionality of the system and may render it computationally intractable without specialized hardware.

5.3.6 Movement Restrictions

Attempts were made to restrict the animals' range of motion by lowering an adjustable roof so they could not stand on their hind legs. This paradoxically reduced prediction accuracy. It may be possible that rats were struggling against the restraints and introducing additional irrelevant neural signals.

It may be possible to design movement restriction that animals will voluntarily comply with. A potential method is requiring rats to press levers after passing a forelimb though a small hole.

5.3.7 Force Distribution Analysis / Gait Lab

Weight of the rat must be distributed between the lever and the cage floor. Therefore pressure sensors could be employed to confirm any change in weight distribution. This could be used to positively identify transition from bipedal to quadruped postures.

REFERENCES

1. Dudchenko, P.A., *An overview of the tasks used to test working memory in rodents*. Neurosci Biobehav Rev, 2004. **28**(7): p. 699-709.

2. Biran, R., D.C. Martin, and P.A. Tresco, *Neuronal cell loss accompanies the brain tissue response to chronically implanted silicon microelectrode arrays.* Exp Neurol, 2005. **195**(1): p. 115-26.

3. Schalk, G., et al., *Two-dimensional movement control using electrocorticographic signals in humans.* J Neural Eng, 2008. **5**(1): p. 75-84.

4. Kubanek, J., et al., *Decoding flexion of individual fingers using electrocorticographic signals in humans.* J Neural Eng, 2009. **6**(6): p. 066001.

5. Iwaniuk, A.N. and I.Q. Whishaw, *On the origin of skilled forelimb movements.* Trends Neurosci, 2000. **23**(8): p. 372-6.

6. Whishaw, I.Q. and B. Gorny, *Does the red nucleus provide the tonic support against which fractionated movements occur? A study on forepaw movements used in skilled reaching by the rat*. Behav Brain Res, 1996. **74**(1-2): p. 79-90.

7. Whishaw, I.Q., B. Gorny, and J. Sarna, *Paw and limb use in skilled and spontaneous reaching after pyramidal tract, red nucleus and combined lesions in the rat: behavioral and anatomical dissociations.* Behav Brain Res, 1998. **93**(1-2): p. 167-83.

8. Murray, H.M. and M.E. Gurule, *Origin of the rubrospinal tract of the rat.* Neurosci Lett, 1979. **14**(1): p. 19-23.

9. ten Donkelaar, H.J., *Evolution of the red nucleus and rubrospinal tract*. Behav Brain Res, 1988. **28**(1-2): p. 9-20.

10. Carmel, J.B., et al., *Feed-forward control of preshaping in the rat is mediated by the corticospinal tract*. Eur J Neurosci, 2010. **32**(10): p. 1678-85.

11. Park, M.C., A. Belhaj-Saif, and P.D. Cheney, *Properties of primary motor cortex output to forelimb muscles in rhesus macaques.* J Neurophysiol, 2004. **92**(5): p. 2968-84.

12. Entakli, J., et al., *TMS reveals a direct influence of spinal projections from human SMAp on precise force production.* Eur J Neurosci, 2013.

13. Conway, B.A., et al., *Synchronization between motor cortex and spinal motoneuronal pool during the performance of a maintained motor task in man.* J Physiol, 1995. **489 (Pt 3)**: p. 917-24.

14. Kilner, J.M., et al., *Task-dependent modulation of 15-30 Hz coherence between rectified EMGs from human hand and forearm muscles.* J Physiol, 1999. **516 (Pt 2)**: p. 559-70.

15. Omlor, W., et al., *Gamma-range corticomuscular coherence during dynamic force output.* Neuroimage, 2007. **34**(3): p. 1191-8.

16. Cheney, P.D., K. Mewes, and E.E. Fetz, *Encoding of motor parameters by corticomotoneuronal (CM) and rubromotoneuronal (RM) cells producing postspike facilitation of forelimb muscles in the behaving monkey.* Behav Brain Res, 1988. **28**(1-2): p. 181-91.

17. Lemon, R.N., G.W. Mantel, and R.B. Muir, *Corticospinal facilitation of hand muscles during voluntary movement in the conscious monkey.* J Physiol, 1986. **381**: p. 497-527.

18. Leenen, L.P., et al., *A detailed morphometrical analysis of the pyramidal tract of the rat.* Brain Res, 1985. **359**(1-2): p. 65-80.

19. Leenen, L.P., et al., *Differences in the fiber composition of the pyramidal tract in two- and 14-month-old rats.* Neuroscience, 1989. **28**(3): p. 635-43.

20. Gorgels, T.G., *A quantitative analysis of axon outgrowth, axon loss, and myelination in the rat pyramidal tract.* Brain Res Dev Brain Res, 1990. **54**(1): p. 51-61.

21. Dunkerley, G.B. and D. Duncan, *A light and electron microscopic study of the normal and the degenerating corticospinal tract in the rat.* J Comp Neurol, 1969. **137**(2): p. 155-83.

22. Mediratta, N.K. and J.A. Nicoll, *Conduction velocities of corticospinal axons in the rat studied by recording cortical antidromic responses.* J Physiol, 1983. **336**: p. 545-61.

23. Casale, E.J., A.R. Light, and A. Rustioni, *Direct projection of the corticospinal tract to the superficial laminae of the spinal cord in the rat.* J Comp Neurol, 1988. **278**(2): p. 275-86.

24. Sasaki, M., et al., *Protection of corticospinal tract neurons after dorsal spinal cord transection and engraftment of olfactory ensheathing cells.* Glia, 2006. **53**(4): p. 352-9.

25. Kwon, B.K., et al., *Survival and regeneration of rubrospinal neurons 1 year after spinal cord injury.* Proc Natl Acad Sci U S A, 2002. **99**(5): p. 3246-51.

26. Schnell, L. and M.E. Schwab, *Sprouting and regeneration of lesioned corticospinal tract fibres in the adult rat spinal cord.* Eur J Neurosci, 1993. **5**(9): p. 1156-71.

27. Prasad, A. and M. Sahin, *Multi-channel recordings of the motor activity from the spinal cord of behaving rats.* Conf Proc IEEE Eng Med Biol Soc, 2006. **1**: p. 2288-91.

28. Prasad, A. and M. Sahin, *Extraction of motor activity from the cervical spinal cord of behaving rats.* J Neural Eng, 2006. **3**(4): p. 287-92.

29. Guo, Y., et al., *Corticospinal signals recorded with MEAs can predict the volitional forearm forces in rats.* Conf Proc IEEE Eng Med Biol Soc, 2013. **2013**: p. 1984-7.

30. Mushahwar, V.K., et al., *Intraspinal micro stimulation generates locomotor-like and feedback-controlled movements.* IEEE Trans Neural Syst Rehabil Eng, 2002. **10**(1): p. 68-81.

31. Mushahwar, V.K., D.F. Collins, and A. Prochazka, *Spinal cord microstimulation generates functional limb movements in chronically implanted cats.* Exp Neurol, 2000. **163**(2): p. 422-9.

32. Hinder, M.R. and T.E. Milner, *The case for an internal dynamics model versus equilibrium point control in human movement.* J Physiol, 2003. **549**(Pt 3): p. 953-63.

33. Ostry, D.J. and A.G. Feldman, *A critical evaluation of the force control hypothesis in motor control*. Exp Brain Res, 2003. **153**(3): p. 275-88.

34. Shadmehr, R. and F.A. Mussa-Ivaldi, *Adaptive representation of dynamics during learning of a motor task.* J Neurosci, 1994. **14**(5 Pt 2): p. 3208-24.

35. Kawato, M., *Internal models for motor control and trajectory planning.* Curr Opin Neurobiol, 1999. **9**(6): p. 718-27.

36. Wolpert, D.M., R.C. Miall, and M. Kawato, *Internal models in the cerebellum.* Trends Cogn Sci, 1998. **2**(9): p. 338-47.

37. Kawato, M., K. Furukawa, and R. Suzuki, *A hierarchical neural-network model for control and learning of voluntary movement*. Biol Cybern, 1987. **57**(3): p. 169-85.

38. Wolpert, D.M. and M. Kawato, *Multiple paired forward and inverse models for motor control.* Neural Netw, 1998. **11**(7-8): p. 1317-1329.

39. Gomi, H. and Kawato, *Equilibrium-point control hypothesis examined by measured arm stiffness during multijoint movement.* Science, 1996. **272**(5258): p. 117-20.

40. Gomi, H. and M. Kawato, *Human arm stiffness and equilibrium-point trajectory during multi-joint movement.* Biol Cybern, 1997. **76**(3): p. 163-71.

41. Corcos, D.M., G.L. Gottlieb, and G.C. Agarwal, *Organizing principles for single-joint movements. II. A speed-sensitive strategy*. J Neurophysiol, 1989. **62**(2): p. 358-68.

42. Gottlieb, G.L., D.M. Corcos, and G.C. Agarwal, *Organizing principles for single-joint movements. I. A speed-insensitive strategy*. J Neurophysiol, 1989. **62**(2): p. 342-57.

43. Franklin, D.W., et al., *Adaptation to stable and unstable dynamics achieved by combined impedance control and inverse dynamics model*. J Neurophysiol, 2003. **90**(5): p. 3270-82.

44. Feldman, A.G. and M.F. Levin, *The equilibrium-point hypothesis--past, present and future*. Adv Exp Med Biol, 2009. **629**: p. 699-726.

45. Feldman, A.G., *Once more on the equilibrium-point hypothesis (lambda model) for motor control*. J Mot Behav, 1986. **18**(1): p. 17-54.

46. Feldman, A.G., et al., *Recent tests of the equilibrium-point hypothesis (lambda model).* Motor Control, 1998. **2**(3): p. 189-205.

47. Adamovich, S.V., M.F. Levin, and A.G. Feldman, *Central modifications of reflex parameters may underlie the fastest arm movements.* J Neurophysiol, 1997. **77**(3): p. 1460-9.

48. Feldman, A.G., S.V. Adamovich, and M.F. Levin, *The relationship between control, kinematic and electromyographic variables in fast single-joint movements in humans.* Exp Brain Res, 1995. **103**(3): p. 440-50.

49. Roberts, W.J., N.P. Rosenthal, and C.A. Terzuolo, *A control model of stretch reflex.* J Neurophysiol, 1971. **34**(4): p. 620-34.

50. Bizzi, E., et al., *Combining modules for movement.* Brain Res Rev, 2008. **57**(1): p. 125-33.

51. Saltiel, P., et al., *Muscle synergies encoded within the spinal cord: evidence from focal intraspinal NMDA iontophoresis in the frog.* J Neurophysiol, 2001. **85**(2): p. 605-19.

52. Tresch, M.C. and E. Bizzi, *Responses to spinal microstimulation in the chronically spinalized rat and their relationship to spinal systems activated by low threshold cutaneous stimulation.* Exp Brain Res, 1999. **129**(3): p. 401-16.

53. Tresch, M.C., P. Saltiel, and E. Bizzi, *The construction of movement by the spinal cord.* Nat Neurosci, 1999. **2**(2): p. 162-7.

54. Giszter, S.F., F.A. Mussa-Ivaldi, and E. Bizzi, *Convergent force fields organized in the frog's spinal cord.* J Neurosci, 1993. **13**(2): p. 467-91.

55. Hogan, N., *The mechanics of multi-joint posture and movement control.* Biol Cybern, 1985. **52**(5): p. 315-31.

56. Bizzi, E., F.A. Mussa-Ivaldi, and N. Hogan, *Regulation of multi-joint arm posture and movement.* Prog Brain Res, 1986. **64**: p. 345-51.

57. Cai, L.Y., Z.Z. Wang, and H.H. Zhang, *[A surface EMG signal identification method based on short-time Fourier transform].* Zhongguo Yi Liao Qi Xie Za Zhi, 2000. **24**(3): p. 133-6.

58. Ong, H.H., et al., *Indirect measurement of regional axon diameter in excised mouse spinal cord with q-space imaging: simulation and experimental studies.* Neuroimage, 2008. **40**(4): p. 1619-32.

59. Webb, A.A. and G.D. Muir, *Unilateral dorsal column and rubrospinal tract injuries affect overground locomotion in the unrestrained rat.* Eur J Neurosci, 2003. **18**(2): p. 412-22.

60. Jarratt, H. and B. Hyland, *Neuronal activity in rat red nucleus during forelimb reach-to-grasp movements.* Neuroscience, 1999. **88**(2): p. 629-42.

61. Belhaj-Saif, A. and P.D. Cheney, *Plasticity in the distribution of the red nucleus output to forearm muscles after unilateral lesions of the pyramidal tract.* J Neurophysiol, 2000. **83**(5): p. 3147-53.

62. Rousche, P.J. and R.A. Normann, *Chronic recording capability of the Utah Intracortical Electrode Array in cat sensory cortex.* J Neurosci Methods, 1998. **82**(1): p. 1-15.

63. Kai, C., *Relationship between Equilibrium Point Control Processes and Electromyographic Pattern in Elbow Joint Movement.* proceedings of the World Congress on Bioengineering, July 2009, Hong Kong, 2009. **Track 3: Biomechanics, Sports Medicine and Rehabilitation**.

64. Lee, Y.Y., et al., *Sustained convergence induced changes in phoria and divergence dynamics.* Vision Res, 2009. **49**(24): p. 2960-72.